Bootstrapping elliptic and Calabi–Yau Feynman integrals

Matthew D. Schwartz
Department of Physics, Harvard University

October 1, 2026

This work is preliminary. Some content remains AI-generated and is still being validated.

Abstract

Over the last two decades, generalized polylogarithmic Feynman integrals went from exotic research problems to core knowledge for scattering amplitudes: the mathematics of iterated integrals, symbols, and canonical differential equations was absorbed and translated by the physics community into a mainstream methodology. Elliptic and Calabi–Yau integrals are the current frontier, but knowledge and methodology are fragmented and not at all standardized. The relevant mathematics runs deep into algebraic and arithmetic geometry, beyond what most physicists are comfortable with. From the bootstrap point of view, however, elliptic integrals have much in common with polylogarithmic ones and can be approached the same way: fix the space of possible answers, cut it down with analytic constraints, pin the last constants, and check everything against values held out from the derivation. The ingredients for the bootstrap change: the function space comes from the geometry of the maximal cut, an elliptic curve or Calabi–Yau manifold in place of an alphabet of logarithms, constraints act on periods, and the boundary constants live in rings set by the geometry's arithmetic, not among the familiar zeta values. The main challenge is that, unlike the polylogarithmic case where mature tools exist at every step, here we had to build much of the toolkit ourselves. Some of it ported straight from mathematics, not yet arrived in physics: Eichler integrals, the Kodaira classification of degenerating elliptic surfaces, the arithmetic of period rings. With these tools the bootstrap yields closed forms for many new integrals. In addition, this approach can yield more general insights such as that the sunrise and banana-family geometry degenerates non-semistably at a mass threshold and that the threshold constants close in classical rings, the lemniscatic $\Gamma(\frac{1}{4})$ ring among them. One worked example, the generic-mass ice-cream cone, is described here; further applications appear in a companion note.

Contents

1 Introduction **3**

2 Periods, monodromy and rings **5**
2.1 The banana family and its periods 5
2.2 Local monodromy and Kodaira fibers 6
2.3 Iterated integrals and the ε-form 7
2.4 Rings of constants and Eichler integrals 7
2.5 The bootstrap for periods 8

3 Degenerations at a mass threshold **8**
3.1 The threshold sunrise . . . 8
3.2 The three-loop banana . . . 10
3.3 Higher loop orders . . . 11
3.4 Cut periods and complete integrals . . . 12

4 Connection coefficients at the threshold **13**
4.1 The spectral projector . . . 13
4.2 Closed forms from the Bessel representation . . . 14
4.3 The unipotent companions . . . 16

5 Complex multiplication **17**
5.1 Frobenius traces and the CM criterion . . . 17
5.2 An inherited-CM obstruction . . . 18
5.3 Quasi-periods and L-values from the operator . . . 19

6 The ice-cream cone **20**
6.1 Kinematics and the integral family . . . 20
6.2 Maximal-cut curves and periods . . . 21
6.3 Landau singularities and the alphabet . . . 22
6.4 The differential equation . . . 23
6.5 Boundary conditions and the closed form . . . 25
6.6 The boundary value as a period . . . 26
6.7 The generic mass point . . . 26
6.8 Order ε . . . 27
6.9 Sequential discontinuities . . . 28
6.10 Numerical comparisons . . . 28

7 Conclusions **30**

A Threshold fibers and operators **31**
A.1 The Type III fiber . . . 31
A.2 Picard–Fuchs operators . . . 32
A.3 Evidence for the K3 label . . . 36

B Further formulas for the ice-cream cone **36**
B.1 Order-ε kernels and cusp data . . . 36
B.2 Ingredients of the boundary integral . . . 37
B.3 The generic-mass boundary vector . . . 37

C Numerical methods and integer-relation searches **38**
C.1 Series solutions and comparisons . . . 38
C.2 The threshold coefficients . . . 39
C.3 Integer-relation searches and point counts . . . 41

1 Introduction

Twenty years of work have turned generalized polylogarithmic Feynman integrals from research problems into a routine part of scattering-amplitude computations. Much of the underlying mathematics, in particular Chen's iterated integrals [25] and Goncharov's multiple polylogarithms with their motivic coproduct [37], predates most of the physics that now relies on it. With the symbol calculus the coproduct became a practical tool for simplifying amplitudes [38], and canonical differential equations reduced the computation of many multi-loop integrals to iterated integration from a boundary value [42, 24]. These methods are now textbook material [29, 43, 66, 69]. Today a physicist computing a polylogarithmic amplitude has a method for every step and rarely consults the mathematical literature.

Elliptic and Calabi–Yau Feynman integrals are the present frontier. The integrals themselves have a long history: the two-loop sunrise graph with massive lines has required elliptic integrals since Sabry's calculation in 1962 [62, 18, 8]. Its higher-loop relatives (the banana graphs) involve a K3 surface at three loops and a Calabi–Yau $(L-1)$-fold at L loops [59, 14, 58]. A common methodology, however, has not yet emerged. The equal-mass sunrise alone has been expressed in terms of elliptic dilogarithms [12], elliptic generalizations of Clausen and Glaisher functions [3], iterated integrals of modular forms [4] and elliptic polylogarithms on the torus [21], and has been computed through dispersion relations [61]. Relating these representations to one another is a research problem in its own right [20] (for reviews see refs. [16, 1]). Moreover, the mathematics underlying these integrals lies deeper in algebraic and arithmetic geometry than the theory of polylogarithms does, and physicists have absorbed much less of it. This mathematics includes degenerations of elliptic surfaces, limiting mixed Hodge structures, complex multiplication (CM) and the modularity of K3 surfaces.

Most of what is known about the sunrise and banana families has been obtained in one of two settings. At the point of maximal unipotent monodromy the Frobenius basis and the methods of mirror symmetry apply [11, 14, 13], and on modular fibrations the integrals are iterated integrals of modular forms [4, 20]. Differential equations in ε-factorized form (with ε the dimensional regulator) are known for the equal-mass sunrise and banana integrals through four loops [4, 59, 58]. At the threshold and pseudo-threshold singularities of the equal-mass banana integrals with an odd loop number the periods have a square-root branch with local monodromy of order two, as shown in refs. [13, 23]. The transcendental lattices of the three-loop banana K3 surfaces have been classified by mass configuration [30], and for three equal masses the maximal cut factorizes into a product of two equal-mass sunrise cuts [32, 31]. The Landau singularities of the two-loop ice-cream cone graph were analyzed in ref. [41], and in two dimensions its top sector has a Picard–Fuchs operator of order two with algebraic solutions [50, 28]. Less attention appears to have been paid to the mass configurations studied here, in which a pseudo-threshold of a banana graph collides with the point of vanishing momentum, and to the periods there.

In this paper we take the bootstrap point of view. By a bootstrap we mean the following procedure. One fixes a space of functions in which the answer must lie and imposes analytic constraints until a few constants remain. These are determined at a boundary point, and the result is compared with numerical values not used in its derivation. For the integrals considered here the space of functions comes from the geometry of the maximal cut (which may be an elliptic curve or a higher-dimensional Calabi–Yau manifold) instead of an alphabet of logarithms. Concretely, in a suitable basis the vector of master integrals I, which depends on a kinematic variable x, satisfies a differential equation in ε-factorized form,

$$\mathrm{d}I(x;\varepsilon) = \varepsilon\, A(x)\, I(x;\varepsilon)\,, \tag{1}$$

in which the entries of A are $\mathrm{d}\log$ forms of algebraic letters together with kernels built from the periods of the maximal cut (for an elliptic curve, its period pair ψ_1, ψ_2; Sec. 2).

The analytic constraints of the bootstrap act on periods. Local exponents and monodromy at the degenerate fibers of the family (together with the regularity of the complete integral there) take the place of first-entry and branch-cut conditions. The degenerate fiber studied here occurs for the $(L{+}1)$-line banana graph with momentum p when the heaviest mass equals the sum of the others,

$$m_{L+1} = m_1 + \cdots + m_L\,, \qquad t = p^2 = 0\,, \tag{2}$$

a mass condition that we refer to as the threshold configuration. We call the point $t = 0$ of the threshold configuration its coalescence point: there the pseudo-threshold $t = (m_{L+1} - \sum_{i\le L} m_i)^2$ meets $t = 0$, whereas the normal threshold $t = (\sum_i m_i)^2$ is a different singular point. The boundary constants that remain to be fixed lie in rings set by the arithmetic of the geometry (in general not zeta values). The mathematical tools we use are the Kodaira classification [49] and Tate's algorithm for the singular fibers, Eichler integrals for quasi-periods and L-values [34], and the Chowla–Selberg formula and Livné's theorem for CM periods [65, 54].

We find that at the coalescence point the local monodromy of the maximal-cut periods of the sunrise and banana graphs is not unipotent. For the two-loop sunrise in the threshold configuration we show that the fiber at $t = 0$ is of Kodaira Type III (an additive fiber with local monodromy of order four); the corresponding elliptic surface is therefore not modular. At three loops the period of the banana K3 surface acquires a half-integer local exponent in addition to a rank-three unipotent block, at a point where the local monodromy is unipotent for generic masses. Through five loops (the last on a single-variable two-mass slice) the finite part of the local monodromy alternates between order four and order two (Sec. 3, Table 1). From the non-oscillatory tail of the Bessel representation we derive in closed form the connection coefficients of the holomorphic period at the coalescence point, that is, its components along the local solutions with fractional exponents (Sec. 4). These coefficients are rational multiples of $\sqrt{3}/\pi$ at three loops, elements of the lemniscatic $\Gamma(\frac{1}{4})$ ring (Laurent polynomials in π and the lemniscate constant with rational coefficients) at four loops, and $\sqrt{2}$ times such elements for the two-loop sunrise. We find numerically that the complete two- and three-loop integrals, unlike their maximal cuts, remain analytic at the coalescence point, and the four-loop master integral evaluated in ref. [64] behaves in the same way.

For the equal-mass and the three-equal-mass three-loop banana graphs, a short argument from the factorization of refs. [32, 31], the lattice classification of ref. [30] and Livné's theorem [54] shows that no non-CM weight-3 period can occur (Proposition 5.1). Finally, we apply the bootstrap to a complete integral, the two-loop ice-cream cone in $d = 2 - 2\varepsilon$ dimensions on a one-scale kinematic slice (Sec. 6). At equal mass we obtain the order-ε^0 top integral in closed form, as a single integral of algebraic kernels against the period pair of its sunrise subgraph. The boundary constants of this closed form are fixed by two conditions at the large-momentum cusp. At one generic mass point (where the cut curve is not modular) we again derive the kernels and the boundary vector, and integrate the top block numerically. The one new constant at equal mass and order ε^0 is a period of the sunrise curve, of transcendental weight three, that matches no classical constant in the rings we searched.

This paper is organized as follows. In Sec. 2 we review the periods of the banana family, their local monodromy and Kodaira fibers, the iterated integrals built on them and the rings of constants that appear, and state the bootstrap in these terms. In Sec. 3 we identify the degenerate fibers at the coalescence point from two through five loops, and in Sec. 4 we derive the connection coefficients of the holomorphic period there. In Sec. 5 we give the CM criterion, prove Proposition 5.1, and recover quasi-periods and L-values from the Picard–Fuchs operator

alone. In Sec. 6 we work through the ice-cream cone from its kinematics to the closed form and its order-ε^1 analog, ending with numerical comparisons. We conclude in Sec. 7. Appendices A–C contain the fiber identifications and operators, further formulas for the cone, and the numerical methods. The reduction to master integrals, the numerical evaluations used for comparison and the software are described in a companion paper [63]. Further integrals computed in the same way, among them four-point functions involving the banana periods studied here, are collected in a companion note [64].

2 Periods, monodromy and rings

In this section we collect the objects used below and fix notation, following refs. [14, 13, 49]; none of the material is new.

2.1 The banana family and its periods

The L-loop banana graph has two vertices joined by $L+1$ massive lines (Fig. 1). The sunrise is its $L=2$ member. With external momentum p and loop momenta $k_1,\dots,k_L$ we define, in $d=2-2\varepsilon$ dimensions [14, 59, 58],

$$I_L(t)=\int\prod_{j=1}^{L}\frac{\mathrm{d}^d k_j}{i\pi^{d/2}}\,\frac{1}{(q^2-m_{L+1}^2)\prod_{j=1}^{L}(k_j^2-m_j^2)}\,,\qquad q=p-\sum_{j=1}^{L}k_j\,,\qquad t=p^2\,,\tag{3}$$

and we write $M_i=m_i^2$. On the maximal cut we take residues loop by loop in the Baikov representation at $d=2$, leaving an $(L-1)$-fold period integral. For the sunrise one variable y survives and the cut is a period of an elliptic curve,

$$\varpi(t)=\oint\frac{\mathrm{d}y}{Y}\,,\qquad Y^2=P(y;t)\,,\tag{4}$$

with $P(y;t)$ a quartic in y, polynomial in t and the M_i (Eq. (15) below). At three loops the cut variety is a one-parameter family of K3 surfaces, and at L loops a family of Calabi–Yau $(L-1)$-folds [14, 13, 47].

The periods are annihilated by the Picard–Fuchs operator obtained from the cut integrand by Griffiths–Dwork reduction [50],

$$L_L\,\varpi=0\,,\qquad L_L=\sum_{k=0}^{n}p_k(t)\,\partial_t^k\,,\tag{5}$$

with polynomial coefficients $p_k(t)$. The singular points of L_L include $t=0$, $t=\infty$, and the thresholds and pseudo-thresholds $t=(m_1\pm m_2\pm\cdots\pm m_{L+1})^2$. All plus signs give the normal threshold. The large-momentum point $z=-1/t=0$ has maximal unipotent monodromy (MUM point), where we normalize the holomorphic period by $\varpi_0=1+O(z)$. At $t=0$ we read the local exponents off the indicial polynomial, the coefficient of the lowest power of t in $L_L\,t^r$. An exponent α isolated modulo $\mathbb{Z}$ gives a power-series solution, and an exponent of multiplicity r_u a logarithmic tower,

$$\Phi_\alpha(t)=t^\alpha(1+O(t))\,,\qquad \Phi^{(k)}(t)=\sum_{j=0}^{k}\frac{\log^j t}{j!}\,t^\alpha f_{k-j}(t)\,,\quad k=0,\dots,r_u-1\,,\tag{6}$$

with $f_0=1+O(t)$ and f_j analytic; $\Phi^{(k)}$ has log depth k. For equal masses $L_3=\mathrm{Sym}^2(L_2)$ up to a change of variable, and the holomorphic K3 period is the square of an elliptic period,

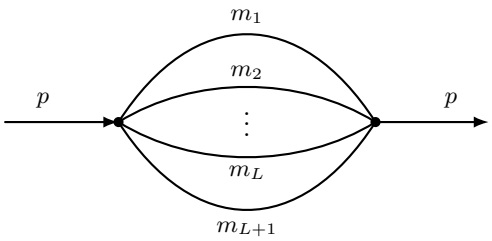

Figure 1: The banana family. Two vertices are joined by $L+1$ internal lines of masses $m_1, \ldots, m_{L+1}$; the external momentum is p, with $t = p^2$, and $L = 2$ is the sunrise. At the threshold configuration $m_{L+1} = m_1 + \cdots + m_L$ of Eq. (2) the pseudo-threshold $t = (m_{L+1} - \sum_{i \le L} m_i)^2$ coincides with $t = 0$; the normal threshold $t = (\sum_i m_i)^2$ is a different point.

with the Domb numbers $1, 4, 28, 256, \ldots$ as Taylor coefficients [59, 14, 47]. Local exponents add under symmetric powers: Sym^{L-1} sends the exponent pair $\{\alpha, \beta\}$ of L_2 at a singular point to $\{(L-1)\alpha,\ (L-2)\alpha + \beta,\ \ldots,\ (L-1)\beta\}$. At $d = 2$ the banana integrals and their cuts have Bessel representations in position space [39, 40, 14], which we use in Sec. 4.

2.2 Local monodromy and Kodaira fibers

Continuing the solutions once around $t = 0$ we obtain the local monodromy $\mathcal{M}_0$, which acts on the basis of Eq. (6) by

$$\Phi_\alpha(e^{2\pi i} t) = e^{2\pi i \alpha}\, \Phi_\alpha(t)\,, \qquad \Phi^{(k)}(e^{2\pi i} t) = e^{2\pi i \alpha} \sum_{j=0}^{k} \frac{(2\pi i)^j}{j!}\, \Phi^{(k-j)}(t)\,, \tag{7}$$

with eigenvalues $e^{2\pi i \alpha}$. By the monodromy theorem (see e.g. ref. [13]) $\mathcal{M}_0$ is quasi-unipotent,

$$\mathcal{M}_0 = \mathcal{M}_s \mathcal{M}_u = \mathcal{M}_u \mathcal{M}_s\,, \qquad \mathcal{M}_s^N = \mathbf{1}\,, \qquad (\mathcal{M}_u - \mathbf{1})^m = 0\,, \tag{8}$$

with $N = 1$ (unipotent) at a MUM point and $m = 1$ (finite order) when all exponents are rational and no logarithm occurs.

For a family of elliptic curves we determine the Kodaira type [49] of the fiber at $t = 0$ from the valuations $v(\cdot)$ of the Weierstrass invariants c_4, c_6 and $\Delta = (c_4^3 - c_6^2)/1728$, by Tate's algorithm; two types occur below,

$$\begin{aligned} I_n:&\quad v(c_4) = 0\,,\ \ v(\Delta) = n\,, && \mathcal{M}_0 \sim \begin{pmatrix} 1 & n \\ 0 & 1 \end{pmatrix}, \\ \mathrm{III}:&\quad v(c_4) = 1\,,\ \ v(c_6) \ge 2\,,\ \ v(\Delta) = 3\,, && \mathcal{M}_0^2 = -\mathbf{1}\,,\quad \mathcal{M}_0^4 = \mathbf{1}\,,\quad j = 1728\,. \end{aligned} \tag{9}$$

Type I_n is multiplicative with unipotent monodromy; Type III is additive (c_4 and c_6 both vanish), with monodromy of order four and j-value 1728, the point of complex multiplication by $\mathbb{Z}[i]$. Of the other additive types only the cuspidal Type II enters below, in Sec. 3.1 and App. A.

A surface with only I_n fibers is called semistable. The sunrise surfaces studied to date are semistable: the equal-mass surface is the universal family over $X_1(6) = \mathbb{H}/\Gamma_1(6)$ with fibers I_2, I_3, I_1, I_6 and a level-six η-quotient as period [12, 4]. For generic masses the four thresholds and pseudo-thresholds carry I_1 fibers [11]. We call a surface modular when t is a Hauptmodul for a torsion-free congruence subgroup Γ and the holomorphic period is a weight-one modular form for

Γ, as in the equal-mass case [20, 67]. The singular fibers of a modular surface lie over the cusps of Γ, each with unipotent shear monodromy up to sign. In particular, a modular surface has no fiber with monodromy of order four; we use this in Sec. 3.1.

Below we continue ϖ_0 from the MUM point to the coalescence point $t = 0$ of the threshold configurations (2) and expand it in the local basis. When the local exponents at $t = 0$ are non-integer values α and one integer of multiplicity r_u, we write

$$\varpi_0(t) = \sum_{\alpha \notin \mathbb{Z}} c_\alpha \, \Phi_\alpha(t) + \sum_{k=0}^{r_u - 1} A_k \, \Phi^{(k)}(t) \,, \tag{10}$$

and call the c_α the connection coefficients and the A_k the unipotent companions. The values of the c_α and A_k quoted in Sec. 4 refer to the rotated local variable $t = e^{-i\pi} s$ defined there.

2.3 Iterated integrals and the ε-form

For a complete integral one can choose master integrals I obeying the ε-form system of Eq. (1) [42]. The matrix A is block lower triangular by sectors. In such a basis each master is normalized by a period of its own sector: ψ_1 for the master of the cut curve, the second-kind quasi-period for its partner, and a third-kind period for a master with a marked point [5, 36, 59]. Let ψ_1, ψ_2 denote the periods of the cut curve (as functions of x), $W = \psi_1 \psi_2' - \psi_1' \psi_2$ their Wronskian, and $\kappa_a(x)$ the algebraic letters of the period-normalized connection. The solutions of Eq. (1) are iterated integrals

$$\widetilde{\Gamma}\Big(a_1 \quad a_2 \quad \cdots \quad a_r\Big)(x) = \int_{x_0}^{x} \kappa_{a_1}(x') \, \widetilde{\Gamma}\Big(a_2 \quad \cdots \quad a_r\Big)(x') \, \mathrm{d}x', \qquad \widetilde{\Gamma}(\,) = 1, \tag{11}$$

with kernels built from the κ_a, ψ_1, ψ_2 and W; every master integral is then a finite combination (with rational-function coefficients) of products $\psi_i \, \widetilde{\Gamma}(\cdots)$.

When the cut curve is modular, as for the equal-mass sunrise on $\Gamma_1(6)$, we pass to $\tau = \psi_2/\psi_1$, which turns the κ_a into modular forms and Eq. (11) into iterated integrals of modular forms with known q-expansions. These iterated integrals can be expressed in terms of the elliptic polylogarithms ELi and $\overline{E}$ [4, 21] on Kronecker–Eisenstein kernels [9], and have a finite symbol alphabet [20, 70]. When the cut curve is not modular there is no such q-expansion, and we keep Eq. (11) in the variable x, with the periods appearing explicitly, as for the sunrise curve of the generic-mass ice-cream cone (Sec. 6). In either case the products $\psi_i \, \widetilde{\Gamma}(\cdots)$ are D-finite. We evaluate them to any precision by series solution of their differential equation from a known value, with rigorous error bounds when the series are summed in ball arithmetic. Public implementations of this series method include `DiffExp` [44] and `SeaSyde` [7]. Where we need numerical values of complete master integrals we take them from `AMFlow` [53].

2.4 Rings of constants and Eichler integrals

The boundary constants below lie in rings determined by the arithmetic of the cut geometry. For the equal-mass banana integrals at the MUM point this ring is the ζ-ring predicted by the $\widehat{\Gamma}$-class [13, 59, 58],

$$\mathcal{R}_\zeta = \mathbb{Q}\big[(2\pi i)^{\pm 1}, \zeta(3), \zeta(5), \dots\big] \,. \tag{12}$$

Two other kinds of ring occur at the coalescence points of Sec. 4: the $\mathbb{Q}$-span of $\sqrt{3}/\pi$ and its products with logarithms of rationals (on the five-loop slice, with $\sqrt{5}/\pi^2$ in place of $\sqrt{3}/\pi$), and the lemniscatic ring. The lemniscatic curve $y^2 = x^3 - x$ has CM by $\mathbb{Z}[i]$ and $j = 1728$, the j-value

of the Type III fiber in Eq. (9). Its real period for $\mathrm{d}x/2y$ is the lemniscate constant ϖ_{lem}, and we define the lemniscatic $\Gamma(\frac{1}{4})$ ring as the Laurent polynomials over $\mathbb{Q}$ in ϖ_{lem} and π,

$$\varpi_{\mathrm{lem}} \;=\; \int_1^\infty \frac{\mathrm{d}x}{\sqrt{x^3-x}} \;=\; 2\int_0^1 \frac{\mathrm{d}t}{\sqrt{1-t^4}} \;=\; \frac{\Gamma(\frac{1}{4})^2}{2\sqrt{2\pi}} \;=\; 2.6220575\ldots, \qquad \mathcal{R}_{\mathrm{lem}} \;=\; \mathbb{Q}[\varpi_{\mathrm{lem}}^{\pm 1},\, \pi^{\pm 1}]. \tag{13}$$

The name refers to Bernoulli's lemniscate $(x^2+y^2)^2 = x^2-y^2$, whose half arc length is ϖ_{lem}. Through $\Gamma(\frac{1}{4})^2 = 2\sqrt{2\pi}\,\varpi_{\mathrm{lem}}$ the monomials of $\mathcal{R}_{\mathrm{lem}}$ become rational monomials in $\Gamma(\frac{1}{4})^{\pm 2}$, $\pi^{\pm 1/2}$ and $\sqrt{2}$, which is the form used in Eq. (41). By the Chowla–Selberg formula, periods of elliptic curves and K3 surfaces with CM are, up to algebraic factors and powers of π, products of Γ-values at rational arguments [65]. The constant ϖ_{lem} is the simplest case, and such a period for $\mathbb{Q}(\sqrt{-15})$ appears in Eq. (59) below.

For a modular form $f(\tau) = \sum_{n\geq 0} a_n q^n$ of weight k (with $q = e^{2\pi i\tau}$) we define the Eichler integral by

$$\widetilde{f}(\tau) = \sum_{n\geq 1} \frac{a_n}{n^{\,k-1}}\, q^n\,, \qquad D^{\,k-1}\widetilde{f} = f - a_0\,, \qquad D = q\,\frac{\mathrm{d}}{\mathrm{d}q} = \frac{1}{2\pi i}\frac{\mathrm{d}}{\mathrm{d}\tau}\,, \tag{14}$$

a $(k-1)$-fold integral of f in τ [34]. It has modular weight $2-k$ up to a period polynomial of degree $k-2$, and is the length-one case of the iterated integrals of modular forms above. In Sec. 5.3 we use two Eichler integrals. The first expresses the equal-mass sunrise quasi-period (proportional to the quasimodular series E_2) through Ramanujan's identity for DE_2; the second is the Eichler integral of the weight-three form of the three-loop banana.

2.5 The bootstrap for periods

The bootstrap set out in the introduction, and in more detail in ref. [63], has, once the family is reduced to master integrals, four steps. First, we take the function space from the cut geometry: the curve or operator of Sec. 2.1 with its periods or Frobenius basis, and the kernels of Eq. (11). Second, we impose the analytic constraints on this space: the local exponents and monodromy at each singular fiber, regularity of the complete integral where the cut degenerates, and the localization of each letter to the sectors of its Landau singularity. Third, we fix the remaining constants analytically at a boundary point, or identify them by an integer-relation search in the appropriate ring of Sec. 2.4. Fourth, we compare the result with numerical evaluations at points used in none of these steps (Sec. 6.10).

3 Degenerations at a mass threshold

When the heaviest mass of a sunrise or banana graph equals the sum of the others, Eq. (2), the maximal cut has two properties at the coalescence point $t = 0$ that we have not found elsewhere in the literature. The sunrise elliptic surface acquires an additive Kodaira fiber there, and through five loops the local monodromy of the cut period has a nontrivial finite part (Table 1).

3.1 The threshold sunrise

The sunrise elliptic surfaces in the literature are semistable: every singular fiber is multiplicative, both for the equal-mass family over $X_1(6)$ [12, 4] and for three distinct masses [11]. At the threshold configuration $\sqrt{M_3} = \sqrt{M_1} + \sqrt{M_2}$, $M_i = m_i^2$, the fiber at $t = p^2 = 0$ becomes instead an additive fiber of Kodaira Type III, with local monodromy of order four, and the surface is then not

modular (Sec. 2.2). We have found no report of an additive Kodaira fiber, or of any non-semistable degeneration, for a sunrise or banana at any mass point.

In the loop-by-loop Baikov representation the sunrise cut is the genus-one curve

$$Y^2 = \lambda(y, M_1, M_2)\,\lambda(t, M_3, y), \qquad \lambda(a,b,c) = a^2 + b^2 + c^2 - 2ab - 2bc - 2ca, \tag{15}$$

whose right-hand side $P(y;t)$ is a binary quartic in the residual cut variable y. A double root of P is a node of the curve and gives a multiplicative I_n fiber; a triple root is a cusp and forces additive reduction. At $t = 0$ the second Källén function is a perfect square, $\lambda(0, M_3, y) = (y - M_3)^2$, and

$$P(y;0) = \lambda(y, M_1, M_2)(y - M_3)^2\,. \tag{16}$$

A triple root forms precisely when $\lambda(M_3, M_1, M_2) = 0$, at the threshold configuration or its pseudo-threshold analog $m_3 = |m_1 - m_2|$.

For the reference point $(M_1, M_2, M_3) = (1, 1, 4)$ we find $P(y;0) = y\,(y-4)^3$. The short Weierstrass model $\eta^2 = \xi^3 + A(t)\,\xi + B(t)$ of the Jacobian of the curve (15) at this point is given by

$$\begin{aligned} A(t) &= -27t^4 + 648t^3 - 3888t^2 - 20736t\,, \\ B(t) &= 54t^6 - 1944t^5 + 23328t^4 - 217728t^3 + 1492992t^2\,, \\ \Delta(t) &\propto t^3(t-16)^2(t-4)^4\,, \qquad (v_{t=0}(c_4), v_{t=0}(c_6), v_{t=0}(\Delta)) = (1,2,3)\,, \end{aligned} \tag{17}$$

so both coefficients vanish at $t = 0$, with the valuation triple of a Type III fiber [49], Eq. (9). From Tate's algorithm we obtain the full configuration of singular fibers,

$$[\,\mathrm{III}\,(t{=}0),\ I_4\,(t{=}4),\ I_2\,(t{=}16),\ I_3\,(t{=}\infty)\,], \tag{18}$$

with Euler numbers summing to 12. The total space is a rational elliptic surface, with an ordinary I_2 fiber at the normal threshold $t = 16$ (Fig. 2). We find the same Type III fiber at $t = 0$ for $(1, 4, 9)$ and $(1, 9, 16)$, with configuration $[\,\mathrm{III}, I_2, I_2, I_2, I_3\,]$, and for the pseudo-threshold point $(4, 9, 1)$. In the family $(1, 1, M)$ with $M \neq 4$ the fiber at $t = 0$ is a multiplicative I_1, as we find at $M = 2, 3, 5, 9$. The Weierstrass coefficients A and B of that family, as polynomials in t and M, have resultant

$$\mathrm{Res}_t(A, B) \propto M^9(M-4)^3\,, \tag{19}$$

whose only non-degenerate zero is $M = 4$.

The local monodromy follows from the Picard–Fuchs equation. By Griffiths–Dwork reduction on the model (17) we obtain, for the period $\Pi = \oint \mathrm{d}\xi/\eta$,

$$\Pi'' + \frac{3t^2 - 40t + 64}{t^3 - 20t^2 + 64t}\,\Pi' + \frac{t^2 - 6t - 4}{t^4 - 20t^3 + 64t^2}\,\Pi = 0\,, \tag{20}$$

with regular singular points at $t = 0, 4, 16, \infty$. Its indicial equation at $t = 0$ and the corresponding Frobenius solutions read

$$r^2 - \tfrac{1}{16} = 0\,, \qquad P_\pm(t) = t^{\pm 1/4}(1 + O(t))\,; \tag{21}$$

the exponents $\pm\frac{1}{4}$ differ by $\frac{1}{2} \notin \mathbb{Z}$ and no logarithm appears. Under $t \to e^{2\pi i}t$ the two solutions acquire the phases $e^{\pm i\pi/2} = \pm i$, and we obtain the local monodromy

$$\mathcal{M}_0 = \mathrm{diag}(i, -i) \ \sim\ S = \begin{pmatrix} 0 & -1 \\ 1 & 0 \end{pmatrix} \in \mathrm{SL}_2(\mathbb{Z}), \qquad S^2 = -\mathbf{1}, \quad S^4 = \mathbf{1}, \tag{22}$$

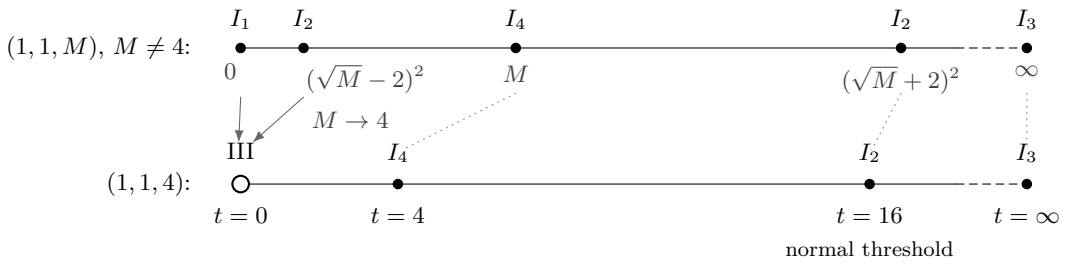

Figure 2: Singular fibers of the $(1,1,M)$ sunrise curve (15) on the t-line: at the threshold configuration $M=4$ (lower row, Eq. (18), positions to scale) the pseudo-threshold fiber has merged with the fiber at $t=0$ into an additive fiber of Kodaira Type III (open circle), while the fiber at the normal threshold $t=16$ remains an ordinary I_2. The upper row shows a generic member of the family, all of whose fibers are multiplicative (filled circles, I_n), with an I_1 fiber at $t=0$ and an I_2 fiber at the pseudo-threshold $t=(\sqrt{M}-2)^2$; its positions are schematic. Here $t=p^2$ and $(1,1,M)$ lists the squared internal masses.

of order four, the monodromy class of a Type III fiber, in place of the unipotent shear $\left(\begin{smallmatrix}1 & n\\ 0 & 1\end{smallmatrix}\right)$ of an I_n fiber. The central fiber has $j(0)=1728$, the j-invariant of the curve with complex multiplication by $\mathbb{Z}[i]$, whose order-four automorphism generates the monodromy. Tate's algorithm applied to a second Weierstrass model of the curve gives the same fiber type (App. A, Table 3). The Type III fiber at the threshold configuration is to our knowledge the first non-semistable degeneration identified for a Feynman elliptic surface.

Type III is also the deepest additive fiber in the family (15). A quadruple root would require the two quadratic factors of P to be proportional, which makes $\Delta \equiv 0$. In a scan over 364 rational mass triples, extended to 936 curves, we find no fiber of Type IV, I_0^*, IV*, III* or II*. Moreover, the triple-root collision forces the valuation $v(c_6)$ to be even, and in particular this family can never reach the cuspidal Type II fiber, whose signature is $v(c_6)$ odd. We do find a Type II fiber on an irreducible cubic pencil outside the family (App. A). Non-modularity is a property of the fibration and not of the fiber at fixed generic t, which is a smooth elliptic curve on which the ε^0 sunrise integral is an elliptic multiple polylogarithm [22]. It obstructs only a global description by iterated integrals of modular forms through $t=0$.

3.2 The three-loop banana

At equal mass the three-loop cut is a family of K3 surfaces whose Picard–Fuchs operator is $L_3 = \mathrm{Sym}^2(L_2)$ [14, 59, 47]. Applied to the threshold sunrise exponents $\{-\frac{1}{4},+\frac{1}{4}\}$ of Eq. (21), the symmetric square would give $\{-\frac{1}{2},0,+\frac{1}{2}\}$, in which the half-integer exponents have eigenvalue -1. The half-integer exponent and the order-two (-1) monodromy of the equal-mass banana K3 are *already* in the literature. As shown in ref. [13], the odd-loop equal-mass bananas have square-root branches at their finite singular points, and ref. [23] gives the local basis there, with exponents $\{0,\frac{1}{2},1\}$ and monodromy $\mathrm{diag}(1,-1,1)$, which is semisimple.

In this paper we extend these results to the unequal-mass threshold configuration. At $\sqrt{M_4}=\sqrt{M_1}+\sqrt{M_2}+\sqrt{M_3}$, with reference point $(M_i)=(1,1,1,9)$ (since $3=1+1+1$), the maximal-cut period satisfies a Picard–Fuchs equation of (order, z-degree) $=(4,5)$ (App. A), whose indicial polynomial and local exponents at $t=0$ are

$$\tfrac{1}{2}\,(r-1)^3(2r-3)\,, \qquad \{1,1,1,\tfrac{3}{2}\}\,, \tag{23}$$

with local monodromy spectrum $\{1,1,1,-1\}$ ($\det = -1$). A $1/t$ pole in the lowest coefficient shows that $t = 0$ is not an apparent singularity. The unit exponents form one unipotent Jordan block of rank three. The Frobenius solution with exponent $\frac{3}{2}$ carries the eigenvalue -1 and has rational coefficients,

$$\Phi_{3/2}(t) = t^{3/2}(1 + \tfrac{19}{216}t + \tfrac{181}{17280}t^2 + \cdots)\,, \tag{24}$$

and we reproduce this eigenvalue by a numerical continuation of the period vector around $t = 0$ (App. A). For generic masses the monodromy there is unipotent. At $(1,1,4,9)$ we find a minimal operator of order five, with exponents $\{1,1,2,2,3\}$ at $t = 0$ and all eigenvalues $+1$; the eigenvalue -1 at $t = 0$ thus requires the coalescence of the pseudo-threshold with that point. A second coalescence, $m_1 + m_4 = m_2 + m_3$ at $(M_i) = (1,4,4,9)$, also produces a half-integer exponent: the minimal operator there has order five, with indicial polynomial and exponents

$$(r-2)(r-1)^3(2r-3)\,, \qquad \{1,1,1,2,\tfrac{3}{2}\} \tag{25}$$

at $t = 0$. There, however, the holomorphic period has no component on the $t^{3/2}$ branch and carries a $\log^2$ term instead, for the parity reason given in Sec. 4.2.

The geometric label of the point $t = 0$ at $(1,1,1,9)$, namely a non-semistable degeneration of the K3 family whose local monodromy has finite part of order two, is strongly supported but not yet certified. We corroborate it with a Baikov double-cover model that has an additive Type III fiber ($v_{t=0}(\Delta) = 3$, $j = 1728$) and Picard–Lefschetz spectrum $\{1,1,1,-1\}$ (App. A), while the order of the finite part is inferred from the period monodromy. At the threshold configuration the known eigenvalue -1 occurs at $t = 0$ together with a unipotent block, whereas at the square-root branch points of the equal-mass family the local monodromy is semisimple. We call a point with such local exponents, here $\{1,1,1,\frac{3}{2}\}$, a point of mixed type. We derive the connection coefficient of ϖ_0 onto the branch (24) in Sec. 4. The banana K3 has been analyzed before [33, 60, 32, 31], at the MUM point or for three equal masses. To our knowledge no Feynman K3 had been expanded around a point of this mixed type, or had a connection coefficient closed onto a fractional branch.

3.3 Higher loop orders

At equal mass the L-loop cut is a Calabi–Yau $(L-1)$-fold [14, 47]. If its operator were the symmetric power $\mathrm{Sym}^{L-1}(L_2)$, as L_3 is up to a change of variable (Sec. 2.1), its local exponents would be sums of those of L_2, and the same power of the threshold sunrise monodromy (22) at the coalescence point would give a local monodromy with finite part

$$\mathrm{Sym}^{L-1}\,\mathrm{diag}(i,-i) \;\sim\; \mathrm{diag}\big(i^{\,L-1},\, i^{\,L-3},\, \ldots,\, i^{-(L-1)}\big)\,, \tag{26}$$

which contains the eigenvalue -1 whenever $L-1$ is even and positive. Its order is therefore

$$\mathrm{ord}(L) = \begin{cases} 4, & L-1 \text{ odd}, \\ 2, & L-1 \text{ even and } \geq 2, \end{cases} \tag{27}$$

that is, $4,2,4,2,\ldots$ for $L = 2,3,4,5,\ldots$. This alternation is the parity statement of ref. [13] ($\mathcal{M}_0 = \mathcal{M}_s\mathcal{M}_u$ as in Eq. (8), with a reflection in $\mathcal{M}_s$ for even fiber dimension), applied at the coalescence point. Away from equal mass the operator is not a symmetric power of L_2 and the argument is heuristic. In Sec. 4.2 we derive the same alternation from the Bessel representation of the period, whose non-oscillatory tail is a series in half-integral inverse powers when the number of propagators is odd and in integral ones when it is even.

L	graph	geometry	mass condition	local data at $t=0$	eig. / ord.	c_α
2	sunrise $(1,1,4)$	elliptic (III)	$\sqrt{4}$=1+1	$(v_{c_4},v_{c_6},v_\Delta)$=(1, 2, 3), j=1728	$\pm i$ / 4	Eq. (43)
3	banana $(1,1,1,9)$	K3	$\sqrt{9}$=1+1+1	$(r-1)^3(2r-3)$	-1 / 2	Eq. (38)
4	banana $(1^4,16)$	CY_3	$\sqrt{16}$=1+1+1+1	$(r-2)^2(r-1)^2(4r-7)(4r-5)$	$\pm i$ / 4	Eq. (41)
5	banana $(1^5,25)$	CY_4	$\sqrt{25}=\sum_1^5 1$	$(r-3)^2(r-2)^3(r-1)^2(2r-3)$	-1 / 2	Eq. (45)

Table 1: Local data of the maximal-cut Picard–Fuchs operator at the coalescence point $t=0$ of the threshold configuration, $L=2,\dots,5$: the finite part of the local monodromy has order $4,2,4,2$, while generic masses give integer exponents at the same point. Columns: the loop order L; the graph with its squared internal masses, where $(1^4,16)\equiv(1,1,1,1,16)$ and $(1^5,25)\equiv(1,1,1,1,1,25)$; the geometry of the cut; the mass condition $m_{L+1}=\sum_{i\le L} m_i$ written in those masses (so $\sqrt{25}=\sum_1^5 1$ abbreviates $\sqrt{25}=1+1+1+1+1$); for $L=2$ the Tate valuations and j-invariant of the fiber, Eq. (17), and for $L\ge 3$ the indicial polynomial of the operator at $t=0$ up to normalization; the non-unit eigenvalues of the local monodromy and the order of its finite part; the equation in which the connection coefficients of the holomorphic period onto the fractional branches are given in closed form. The CY_4 row is computed on a single-variable two-mass slice of the multinomial-squared period of ref. [14]; no five-loop graph realizing this slice as a normal threshold has been exhibited, so its reading as a physical-threshold rung is conjectural, by analogy with the lower rungs.

We confirm the alternation of the monodromy order through five loops from the exact indicial polynomials of the threshold operators (Table 1). We obtain these operators without solving any master integral, from a nullspace fit to the multinomial-squared period series of ref. [14] modulo 31-bit primes with rational reconstruction. We find (order, z-degree) $=(4,5)$ for the K3, $(6,9)$ for the CY_3 and $(8,14)$ for the CY_4 operator ($(5,11)$, $(6,9)$ and $(8,16)$ for generic masses), with zero annihilation residual (App. A). The $L=5$ operator is computed on a single-variable two-mass slice of the multinomial-squared period, with no five-loop graph yet exhibited that realizes the slice as a normal threshold.

Beyond the alternation, we find a point of mixed type at $t=0$ and, at four loops, a pair of quarter-integer exponents. At the CY_3 point $(1,1,1,1,16)$ we find the indicial polynomial

$$(r-2)^2(r-1)^2(4r-7)(4r-5) \tag{28}$$

at $t=0$, with exponents $\{\frac{5}{4},\frac{7}{4}\}$, whose eigenvalues $\pm i$ have order four, together with a unipotent block of rank four. The equal-mass four-loop operator has integer exponents at every singular point [13, 14], and this pair therefore arises from the coalescence of the pseudo-threshold with $t=0$, whereas the unequal-mass analysis of ref. [55] is carried out at the MUM point. Singular points whose monodromy has finite order, with fractional exponents such as $\{0,\frac{1}{4},\frac{3}{4},1\}$, occur in the database of Calabi–Yau operators [6, 68] and at Gepner points [48], but not, so far as we have found, at the physical threshold of a Feynman family.

3.4 Cut periods and complete integrals

The finite part of the local monodromy at the coalescence point is carried by the homogeneous solutions of the differential equations, that is, by the cut periods. The complete integrals, which solve the inhomogeneous system, are analytic at the coalescence point in every case where we could compute them. For the $(1,1,4)$ sunrise, `AMFlow` evaluations [53] of the master integral $I[1,1,1]$ (unit propagator powers) at ten Euclidean points near $t=0$ are reproduced by an integer-power

Taylor series for the ε^0 coefficient,

$$M^{(0)}(t) = -2\log 2 + a_1 t + \cdots . \tag{29}$$

When we include terms $t^{1/4}$ and $t\log t$ in the fitted series, their coefficients are consistent with exactly zero (App. C). The two fractional solutions $P_\pm$ of Eq. (21) cancel in the combination that the boundary conditions select. We find likewise that the three-loop master $I[1,1,1,1]$ at $(1,1,1,9)$, sampled at nine Euclidean points, is analytic at $t=0$, while the cut period carries the $t^{3/2}$ branch. Complete four-point integrals in which the equal-mass banana K3 period enters at order ε^0 are treated in ref. [64]. At four loops the top master integral of the $(1,1,1,1,16)$ family at $d=2$, evaluated by auxiliary mass flow at two Euclidean points in ref. [64], is likewise analytic at $t=0$: the coefficients of its $t^{5/4}$ and $t^{7/4}$ branches are bounded by 10^{-23} and no logarithm appears (App. C). At five loops the question is untested, because no five-loop unequal-mass master solve exists.

Near the coalescence point, a fit of the cut period to the values of the holomorphic Sym^{L-1}-of-sunrise solutions does not determine its fractional component (App. C.2). We therefore integrate the Picard–Fuchs equation through the point (Sec. 4.1), and in Sec. 4.2 we derive the connection coefficients in closed form.

The distinction between unipotent and non-unipotent monodromy has a physical interpretation, offered here as a falsifiable prediction, not a value-fit. Periods of unipotent degenerations, with $\mathcal{M}_0 - \mathbf{1}$ nilpotent, cancel in conservative observables, while periods of non-unipotent degenerations, with $\mathcal{M}_0 - \mathbf{1}$ invertible, survive in dissipative ones. We have worked out one example, at a different point from $t=0$: the four-particle normal threshold $t_{\mathrm{thr}} = (\sum_i m_i)^2$ of the three-loop banana. There the $d=4$ four-body phase space opens as $(t-t_{\mathrm{thr}})^{7/2}$, with eigenvalue -1, verified numerically to five digits. Like the cut exponent $\frac{3}{2}$, this exponent lies in $\frac{1}{2}+\mathbb{Z}$. The $t^{1/4}$ branch of the sunrise cut, by contrast, is not a phase-space edge, since a three-body cut opens with an integer power. That the half-integer edge survives into a physical dissipative observable is the prediction.

4 Connection coefficients at the threshold

In this section we determine the connection coefficients c_α of Eq. (10) in closed form, together with the unipotent companions A_k. They connect the holomorphic period ϖ_0, normalized by $\varpi_0 = 1 + O(z)$ at the MUM point, to the local solutions at the coalescence points of Table 1.

4.1 The spectral projector

Solving for c_α in the full local Frobenius basis is an ill-conditioned linear problem, because the unipotent logarithmic tower enters every component of the numerically continued solution vector with terms $\sim 10^4$ larger than the fractional branch. Instead we project onto the fractional branch algebraically. The local monodromy $\mathcal{M}_0$ at $t=0$ is the product of a unipotent block of rank r_u, with nilpotency index at most r_u, and a semisimple block with distinct eigenvalues $\{\lambda\}$ of finite order. We define

$$P_\lambda \;=\; \frac{1}{N_\lambda}\,(\mathcal{M}_0 - \mathbf{1})^{r_u} \prod_{\mu\neq\lambda} (\mathcal{M}_0 - \mu\mathbf{1})\,, \qquad N_\lambda \;=\; (\lambda-1)^{r_u} \prod_{\mu\neq\lambda} (\lambda-\mu)\,. \tag{30}$$

The operator P_λ annihilates the unipotent block, on which $(\mathcal{M}_0 - \mathbf{1})^{r_u} = 0$, and every eigenvector with eigenvalue $\mu \neq \lambda$; on the one-dimensional λ-eigenspace it is the identity. Acting on the local

components of ϖ_0 it isolates $c_\alpha \Phi_\alpha$ (with λ and α related by Eq. (7)). At the three-loop point $(M_i) = (1,1,1,9)$ we have $r_u = 3$ and $\lambda = -1$, which gives

$$P_{-1} = -\tfrac{1}{8}(\mathcal{M}_0 - \mathbf{1})^3\,, \qquad P_{-1}\,\varpi_0 = c_{3/2}\,\Phi_{3/2}\,. \tag{31}$$

We read the eigenvalues entering Eq. (30) off the factored indicial polynomials of Table 1. We obtain $\mathcal{M}_0$ and the local components of ϖ_0 by numerical continuation of the Picard–Fuchs equation around $t = 0$ (App. C.2).

4.2 Closed forms from the Bessel representation

The coefficients c_α also follow analytically from the position-space Bessel representation of the banana periods [39, 40, 14, 19]. We take the four-loop point $(M_i) = (1,1,1,1,16)$ as the example. In what follows s denotes the invariant p^2, continued through the upper half-plane from the region beyond the normal threshold, where the Bessel representation below converges. The corresponding local variable at the coalescence point is $t = e^{-i\pi}s$; it is positive for Euclidean momenta and differs in sign from the variable $t = p^2$ of Sec. 3. For $\sqrt{s} > 8$ the holomorphic period is given by

$$\varpi_0(s) = s\int_0^\infty x\,K_0(\sqrt{s}\,x)\,I_0(x)^4 I_0(4x)\,\mathrm{d}x\,, \tag{32}$$

(normalization $\varpi_0 = 1 + O(z)$), and the rotation $x = -iy$ gives

$$\varpi_0(s) = -\tfrac{i\pi}{2}\,s\int_0^\infty y\,H_0^{(1)}(\sqrt{s}\,y)\,J_0(y)^4 J_0(4y)\,\mathrm{d}y\,, \qquad \mathrm{Im}\,s \geq 0\,, \tag{33}$$

with one factor $J_0(m_i y)$ for each of the five lines. Fractional powers of s at $s \to 0$ come only from the non-oscillatory tail of the Bessel product at large y. This tail is the cross term of the five large-argument asymptotics with signed frequencies $(+4,-1,-1,-1,-1)$, which does not oscillate because these frequencies sum to zero precisely when $m_5 = m_1 + m_2 + m_3 + m_4$. For the kernel $J_0(y)^4 J_0(4y)$ the tail reads

$$J_0(y)^4 J_0(4y) \supset -(8\pi^{5/2})^{-1} y^{-5/2}(1 + \tfrac{15}{32}y^{-1} + \dots)\,. \tag{34}$$

Each tail term is integrated using the Mellin formula

$$\int_0^\infty y^{\lambda-1} H_0^{(1)}(\mu y)\,\mathrm{d}y = \tfrac{2}{i\pi}\,2^{\lambda-2}(-i\mu)^{-\lambda}\Gamma(\lambda/2)^2\,, \tag{35}$$

which converges for $\mathrm{Re}\,\lambda > 0$ (with $\mathrm{Im}\,\mu > 0$) and is continued to negative λ through its Γ factors, with $\mu = \sqrt{s}$.

With N Bessel factors the non-oscillatory tail is a sum of powers $y^{-N/2-n}$ (integer $n \geq 0$). A tail term $a\,y^{-N/2-n}$ of the Bessel product in Eq. (33) is integrated by Eq. (35) at $\lambda = 2 - N/2 - n$, and with $s(-i\sqrt{s})^{2\alpha-2} = -t^\alpha$ on the branch $t = e^{-i\pi}s$ we obtain

$$-\tfrac{i\pi}{2}\,s\int_0^\infty y\,H_0^{(1)}(\sqrt{s}\,y)\;a\,y^{-N/2-n}\,\mathrm{d}y \;=\; a\,2^{-2\alpha}\,\Gamma(1-\alpha)^2\,t^\alpha\,, \qquad \alpha = \frac{N}{4} + \frac{n}{2}\,. \tag{36}$$

Summed over the tail, the right-hand side is the fractional part $\sum_\alpha c_\alpha \Phi_\alpha(t)$ of Eq. (10): the lowest power on each branch gives $c_\alpha = 2^{-2\alpha}\Gamma(1-\alpha)^2\,a$, and the higher powers reproduce the Frobenius expansions of the Φ_α. When α is an integer, $\Gamma(1-\alpha)^2$ has a double pole and the tail term produces logarithms instead. At the second coalescence $(M_i) = (1,4,4,9)$, where $m_1 + m_4 = m_2 + m_3$, the

tail of $J_0(y)J_0(2y)^2J_0(3y)$ has even inverse powers only, so that ϖ_0 carries a $\log^2$ term there and has no component on the $t^{3/2}$ branch. Quarter-integer exponents, and with them $\Gamma(\frac{1}{4})^2$ and $\Gamma(\frac{3}{4})^2$, likewise occur exactly when N is odd, that is, at the loop orders $L = 2, 4, \ldots$, where the finite part of the monodromy has order four by Eq. (27). For even N the exponents are half-integers and $\Gamma(-\frac{1}{2} - k)^2 \in \mathbb{Q}\,\pi$, which together with the radical $(\prod_i m_i)^{-1/2}$ of the tail gives the $\sqrt{3}/\pi$ ring at three loops and the $\sqrt{5}/\pi^2$ ring on the CY_4 slice. We expect this parity rule to persist at all loop orders.

At the three-loop point $(M_i) = (1, 1, 1, 9)$ the Bessel product is $J_0(y)^3J_0(3y)$, whose tail has odd inverse powers only,

$$J_0(y)^3 J_0(3y) \supset -\frac{\sqrt{3}}{18\pi^2}\, y^{-3} + \frac{19\sqrt{3}}{432\pi^2}\, y^{-5} - \cdots . \tag{37}$$

For the y^{-3} term we have $\alpha = \frac{3}{2}$, and Eq. (36) gives

$$c_{3/2} \;=\; -\frac{\sqrt{3}}{36\,\pi}\,. \tag{38}$$

Here 36 is the normal-threshold momentum squared. The projection (31) of the numerically continued period reproduces Eq. (38) in ball arithmetic to 195 digits (Table 2). From the y^{-5} term we obtain the subleading power on the same branch,

$$\frac{19\sqrt{3}}{7776\pi}\, t^{5/2} = c_{3/2} \cdot (-\tfrac{19}{216}) t^{5/2}\,, \tag{39}$$

which is the next term of the Frobenius expansion of $\Phi_{3/2}$. In Eq. (24) the same branch is written in $t = p^2$, and its odd-order coefficients therefore have the opposite sign.

At the four-loop point the local monodromy spectrum is $\{1^4, +i, -i\}$ ($r_u = 4$), and $(\mathcal{M}_0 - \mathbf{1})^4$ removes the unipotent block and acts as $(\pm i - 1)^4 = -4$ on the semisimple pair; the projectors (30) are

$$P_{+i} \;=\; \tfrac{i}{8}\,(\mathcal{M}_0 - \mathbf{1})^4(\mathcal{M}_0 + i\mathbf{1})\,, \qquad P_{-i} \;=\; -\tfrac{i}{8}\,(\mathcal{M}_0 - \mathbf{1})^4(\mathcal{M}_0 - i\mathbf{1})\,. \tag{40}$$

From the two tail terms of Eq. (34), with $\alpha = \frac{5}{4}$ and $\frac{7}{4}$ (Mellin exponents $\lambda = -\frac{1}{2}, -\frac{3}{2}$ in Eq. (35)), we obtain by Eq. (36) $c_{5/4} = -(8\pi^{5/2})^{-1}2^{-5/2}\Gamma(-\frac{1}{4})^2$ and $c_{7/4} = -\frac{15}{32}(8\pi^{5/2})^{-1}2^{-7/2}\Gamma(-\frac{3}{4})^2$, that is

$$\boxed{\;c_{5/4} \;=\; -\frac{1}{\sqrt{2\pi}\,\Gamma(\frac{1}{4})^2} \;=\; -\frac{\Gamma(\frac{3}{4})^2}{2\sqrt{2}\,\pi^{5/2}}\,, \qquad c_{7/4} \;=\; -\frac{5\,\Gamma(\frac{1}{4})^2}{384\sqrt{2}\,\pi^{5/2}}\,,\;} \tag{41}$$

with the product

$$c_{5/4}\, c_{7/4} \;=\; \frac{5}{768\,\pi^3}\,, \qquad 768 = 12 \cdot \big(\textstyle\sum_i \sqrt{M_i}\big)^2. \tag{42}$$

The product identity follows from $\Gamma(\frac{1}{4})\Gamma(\frac{3}{4}) = \pi\sqrt{2}$ and expresses the Wronskian normalization of the conjugate $\{+i, -i\}$ pair. In the period presentation of the lemniscatic ring (13) the coefficients read $c_{5/4} = -1/(4\pi\varpi_{\mathrm{lem}})$ and $c_{7/4} = -5\,\varpi_{\mathrm{lem}}/(192\pi^2)$. Both are elements of $\mathcal{R}_{\mathrm{lem}}$. The projections (40) of the numerically continued period reproduce the two coefficients in ball arithmetic to 197 digits (Table 2). Auxiliary mass flow does not apply to a connection coefficient, so there is no such evaluation of $c_{5/4}$ and $c_{7/4}$ themselves; ref. [64] recovers their first 45 digits from the maximal-cut operator of the family's own nine-master reduction, and evaluates the complete master integral of the family at $d = 2$ by auxiliary mass flow (Sec. 3.4).

The lemniscate constant ϖ_{lem} is already present at two loops. The $(1, 1, 4)$ holomorphic period $\varpi_0 = 1 + O(z)$, continued from the MUM point to the coalescence point of its Type III fiber,

has local exponents $\{\frac{3}{4},\frac{5}{4}\}$ there, the exponents $\pm\frac{1}{4}$ of Eq. (21) up to the integer shift from the normalization of the period. It equals $c_{3/4}\Phi_{3/4}+c_{5/4}\Phi_{5/4}$, with a coefficient $c_{5/4}$ unrelated to the four-loop one. Repeating the computation with three Bessel factors, we find

$$c_{3/4} \;=\; \frac{\Gamma(\frac{1}{4})^2}{8\,\pi^{3/2}} \;=\; \frac{\sqrt{2}\,\varpi_{\rm lem}}{4\pi}\,, \qquad c_{5/4} \;=\; -\,\frac{3\,\Gamma(\frac{3}{4})^2}{16\,\pi^{3/2}} \;=\; -\,\frac{3\sqrt{2}}{32\,\varpi_{\rm lem}}\,, \qquad c_{3/4}\,c_{5/4} \;=\; -\,\frac{3}{64\,\pi}\,, \tag{43}$$

in agreement with the numerical continuation of the second-order operator in ball arithmetic to 159 digits (Table 2). At two and at four loops $\varpi_{\rm lem}$ enters as a local connection coefficient of the holomorphic period rather than as a boundary L-value.

Similarly, on the two-mass CY_4 slice $(1^5,25)$ of Table 1 ($r_u=7$, eigenvalue $\lambda=-1$, $P_{-1}=-\frac{1}{128}(\mathcal{M}_0-\mathbf{1})^7$) six Bessel factors again give odd inverse powers only,

$$J_0(y)^5 J_0(5y) \supset -\frac{1}{4\sqrt{5}\,\pi^3}\,y^{-3}+\cdots\,, \tag{44}$$

whose leading term has $\alpha=\frac{3}{2}$ and gives, by Eq. (36),

$$c_{3/2} \;=\; -\,\frac{\sqrt{5}}{40\,\pi^2}\,. \tag{45}$$

From the subleading tail term we obtain the ratio of the $t^{5/2}$ and $t^{3/2}$ coefficients as $-\frac{11}{200}$, the next Frobenius coefficient of $\Phi_{3/2}$ on the slice. The projected period agrees with Eq. (45) to 248 digits in ball arithmetic (Table 2). The coefficient (45) lies in the $\sqrt{5}/\pi$ analog of the three-loop ring, with π^{-2} in place of π^{-1} ($|c_{3/2}|^2=1/(320\pi^4)$), although here the denominator 40 is not the normal-threshold momentum squared 100 (compare the 36 of Eq. (38)).

4.3 The unipotent companions

The projector isolates the fractional branches; the complementary data are the coefficients A_k of Eq. (10) on the unipotent tower. At the three-loop point the tower is $\{\Phi^{(0)},\Phi^{(1)},\Phi^{(2)}\}$ (log depth $0,1,2$), and in the branch convention $t=e^{-i\pi}s$ we find

$$A_0=\frac{\sqrt{3}\,\log 24}{12\pi}\,, \qquad A_1=-\frac{\sqrt{3}}{24\pi}=\tfrac{3}{2}\,c_{3/2}\,, \qquad A_2=0\,. \tag{46}$$

We can prove the values of A_2 and A_1 analytically. Indeed, the tail (37) has odd inverse powers only, because its coefficients are the real parts of $i^{\,n+1}$ times rationals. The corresponding Mellin exponents $\lambda=-n$ are then odd, and $\Gamma(\lambda/2)^2$ is finite at odd λ; no tail term meets a double pole of $\Gamma(\lambda/2)^2$, and the expansion of ϖ_0 at $t=0$ has no $t\log^2 t$ term at any order. Hence A_2 vanishes identically. The $s\log s$ term comes only from the small-argument logarithm of $H_0^{(1)}$, with coefficient $\frac{1}{2}\int_0^\infty y\,J_0(y)^3J_0(3y)\,\mathrm{d}y$. This moment is Kluyver's three-step random-walk integral at the endpoint of the walk's range,

$$\int_0^\infty y\,J_0(y)^3J_0(3y)\,\mathrm{d}y=\frac{p_3(3)}{3}=\frac{\sqrt{3}}{12\pi}\,, \tag{47}$$

with the density $p_3(3)$ taken as the mean of its one-sided limits [15], and it gives the value of A_1 in Eq. (46).

For A_0 the small-argument expansion of the Hankel form gives

$$A_0=-\int_0^\infty y\log y\,J_0(y)^3J_0(3y)\,\mathrm{d}y-(\gamma_E-\log 2)\,\tfrac{\sqrt{3}}{12\pi}\,, \tag{48}$$

and the closed form in Eq. (46) is therefore equivalent to the moment evaluation

$$\int_0^\infty y \log y \, J_0(y)^3 J_0(3y) \, \mathrm{d}y = -\sqrt{3}\,(\log 12 + \gamma_E)/(12\pi)\,, \tag{49}$$

which we have not proved. We have confirmed Eq. (49) numerically, by direct integration to 34 digits, and the numerical continuation of the operator in ball arithmetic gives A_0 of Eq. (46) to 153 digits (Table 2). On the branch $t = e^{-i\pi}s$ the unipotent part of ϖ_0 is thus

$$A_0\,\Phi^{(0)} + A_1\,\Phi^{(1)} = \tfrac{3}{2}c_{3/2}(\Phi^{(1)} - 2\log(24)\,\Phi^{(0)}), \tag{50}$$

and the natural logarithmic variable is $\log(t/576)$. All three companions lie in the $\mathbb{Q}$-span of $\sqrt{3}/\pi$ and its products with logarithms of rationals (Sec. 2.4), as does $c_{3/2}$.

At four loops the unipotent block has rank four. It consists of two analytic solutions, $\Phi_1 = t + O(t^3)$ (no t^2 term) and $\Phi_2 = t^2(1 + O(t))$, each with a logarithmic partner. The coefficients of ϖ_0 on both logarithmic partners vanish,

$$\varpi_0 = c_{5/4}\Phi_{5/4} + c_{7/4}\Phi_{7/4} + \alpha_1\Phi_1 + \alpha_2\Phi_2\,, \qquad \alpha_1 = 0.1120550986\ldots, \quad \alpha_2 = -0.001640947945\ldots, \tag{51}$$

where we obtain α_1 and α_2 from the numerical continuation of the operator (App. C.2). The small-argument expansion of the Hankel form gives $\alpha_1 = -\int_0^\infty y \log y \, J_0(y)^4 J_0(4y)\,\mathrm{d}y$ (the two sides agree to 35 digits by direct integration). The $s \log s$ term is absent because $\int_0^\infty y\, J_0(y)^4 J_0(4y)\,\mathrm{d}y = 0$: the four-step random-walk density vanishes at the endpoint of its range [15]. The vanishing of the second logarithmic coefficient remains a numerical statement (App. C.2).

5 Complex multiplication

The connection coefficients of Sec. 4 lie in elementary rings such as the $\mathbb{Q}$-span of $\sqrt{3}/\pi$, or in the lemniscatic ring (13). The boundary constants of the equal-mass banana periods and integrals are ζ-values or CM Γ-periods. A non-CM weight-3 motive would instead have two transcendental periods, conjecturally algebraically independent. We ask whether the banana family contains such a motive. For the equal-mass and the three-equal-mass three-loop banana, the two configurations analyzed here, the answer is no.

5.1 Frobenius traces and the CM criterion

We write a_p for the Frobenius trace of a smooth fiber X_t, computed from its number of $\mathbb{F}_p$-points. For a singular K3 (one of maximal Picard rank) the trace on the transcendental lattice $T(X_t) \subset H^2$ is the Fourier coefficient of the associated weight-3 newform. Such a newform f has CM by an imaginary-quadratic field K of discriminant d_K precisely when

$$a_p(f) = 0 \qquad \text{for every prime } p \text{ with } \left(\tfrac{d_K}{p}\right) = -1\,, \tag{52}$$

i.e. at the primes inert in K.

For the sunrise the second Symanzik polynomial defines the pencil of cubics

$$F \;=\; -\,t\,x_1x_2x_3 \;+\; (M_1x_1 + M_2x_2 + M_3x_3)(x_1x_2 + x_2x_3 + x_3x_1), \qquad M_i = m_i^2, \tag{53}$$

whose total space $S \to \mathbb{P}^1_t$ is an elliptic surface with $e(S) = 12$, hence $\chi(\mathcal{O}_S) = 1$ and $p_g = h^{2,0} = 0$. With no holomorphic two-form there is no weight-3 cusp form on this surface. At equal

mass the weight-3 modular forms that enter the sunrise integral are Eisenstein series [4, 20], and the holomorphic period is the weight-one form of Sec. 2.2. Our point counts show no cusp-form contribution. We find the same fibral trace sum $\sum_t a_{E_t}(p) = -3p - 1$ at every prime $5 \le p \le 199$ for each of the ten mass triples counted.

A weight-3 cusp form first appears at three loops, where the maximal cut is a K3 with $e = 24$ and $p_g = 1$ [59, 32]. At equal mass its Picard–Fuchs operator is the symmetric square of the sunrise operator, and the K3 at the on-shell point is singular, with transcendental lattice of rank two. Its newform is

$$f_3 = 15.3.\text{b.a} = (\eta_3\eta_5)^3 + (\eta_1\eta_{15})^3\,, \qquad \eta_N = \eta(N\tau)\,. \tag{54}$$

Counting points, we find that a_p vanishes at 23 of the 44 unramified primes $p \le 200$ (zero density 0.523, against the Chebotarev value $\frac{1}{2}$), following the inert-prime law

$$a_p = 0 \iff \left(\tfrac{-15}{p}\right) = -1, \qquad \text{at every unramified prime } p \le 200. \tag{55}$$

The point counts thus display, through the criterion (52), the classical CM of f_3 by $\mathbb{Q}(\sqrt{-15})$. By contrast, the smallest non-CM weight-3 newform, 12.3.d.a with coefficient field $\mathbb{Q}(\sqrt{-3})$, has $a_p = 0$ at one of the first 168 primes (the lone $a_{71} = 0$), a zero density of 0.006 against 0.523 for f_3.

5.2 An inherited-CM obstruction

For unequal masses the transcendental lattice of the three-loop banana cut, of rank four to six, and the modular forms parametrizing its periods are given in ref. [30] as

$$T(X) \;\cong\; \begin{cases} H \oplus H(3) & \text{three equal masses (ordinary modular forms in two variables),} \\ H \oplus \langle 2\rangle \oplus \langle -6\rangle & \text{pairwise-equal masses (Hilbert modular forms over } \mathbb{Q}(\sqrt{3})), \\ H \oplus H \oplus \langle -6\rangle & \text{two equal masses (Siegel modular forms),} \\ H \oplus H \oplus A_2(-3) & \text{four different masses (Hermitian modular forms).} \end{cases} \tag{56}$$

As shown in refs. [32, 31], the three-equal-mass periods are products of two copies of the equal-mass sunrise maximal cut, with two independent moduli τ_1, τ_2 on $\Gamma_1(12) \times \Gamma_1(12)$.

Proposition 5.1 (inherited-CM obstruction)**.** *The three-equal-mass three-loop banana K3, with transcendental lattice $H \oplus H(3)$, has a maximal cut equal to the product of two copies of the equal-mass sunrise maximal cut. Its weight-3 arithmetic is therefore that of the equal-mass sunrise family, whose CM fiber carries f_3 with CM by $\mathbb{Q}(\sqrt{-15})$, and neither the equal-mass nor the three-equal-mass three-loop banana can realize a non-CM weight-3 Feynman number.*

Proof. By the factorization [32, 31], the transcendental motive of the three-equal-mass K3 is assembled from two members of the equal-mass sunrise family, and its weight-3 arithmetic is therefore that of one elliptic family over $\mathbb{Q}$. The Frobenius traces are rational, whereas a non-CM weight-3 newform has coefficient field of degree ≥ 2. At the fiber where both factors sit at the CM point (the equal-mass limit) the weight-3 piece is f_3 of Eq. (54), with CM by $\mathbb{Q}(\sqrt{-15})$ (Eq. (55)). A motive assembled by tensor or symmetric construction from CM pieces is itself CM. The weight-3 number produced there is therefore a CM Γ-period. At equal mass the transcendental lattice has rank two and the K3 is singular. By Livné's modularity theorem [54] its transcendental L-function is that of a weight-3 newform with CM by an imaginary-quadratic field, here f_3. Hence neither configuration realizes a non-CM weight-3 period. □

The proposition is exactly as strong as its ingredients, so we state their status. The factorization is a theorem of refs. [32, 31]; the lattices are those of ref. [30]; the CM of f_3 is classical (Eq. (55)); the closure step is elementary. Our toric point count (App. C.3) shows the same CM pattern, but the conclusion follows from the proposition, which does not rely on the point count. This rules out the equal-mass and three-equal-mass rungs, and only those. For unequal masses the rank of $T(X)$ in Eq. (56) exceeds two, and a non-CM weight-3 newform could occur only as a Galois-conjugate pair of rank-two pieces. Whether the Hilbert-modular pairwise-equal banana contains such a non-CM pair is not settled by the factorization argument, which applies to three equal masses only, and the records of this program do not analyze it.

Two candidate homes remain in the records, neither analyzed to a verdict. One is the pairwise-equal banana. The other is a graph whose maximal-cut surface carries a nebentypus character on its transcendental H^2, as do the elliptic modular surfaces attached to weight-3 newforms with imaginary-quadratic coefficients. The two-curve geometries we examined [57, 71] have non-CM curves but rational-integer Frobenius traces, and realize weight-2 and weight-4 modular forms without such a character. The question of a non-CM weight-3 period thus has a negative answer for the configurations of Proposition 5.1; for the pairwise-equal banana and for a character-carrying surface it is open.

5.3 Quasi-periods and L-values from the operator

A representation of the periods by Eichler integrals (14) involves a quasi-period and a boundary constant. We find that both follow from the Picard–Fuchs operator alone. For the equal-mass sunrise the quasi-period is

$$\Pi_2(t) = (\pi^2/3)E_2(\tau_F)\,, \tag{57}$$

with τ_F the modular parameter of the fiber, and by Ramanujan's identity

$$\mathrm{D}E_2 = (E_2^2 - E_4)/12\,, \qquad \mathrm{D} = q\,\frac{\mathrm{d}}{\mathrm{d}q}\,, \tag{58}$$

E_2 is, up to its constant term, the onefold integral D^{-1} of a weight-4 quasimodular form. At five Euclidean points we recover its constant of integration and normalization (both equal to 1) by an integer-relation search among Π_2, this integral and unity. The relation holds to 99 digits at the worst point, against two digits for a fit to holomorphic modular forms.

The boundary constant of the Eichler integral is a critical L-value, determined by the Frobenius traces, which in turn follow from the operator: for the $(1,1,4)$ surface the truncated p-adic Frobenius of the operator reproduces a_p at every prime we tested. For f_3 we then identify $L(f_3,2)$, by integer-relation search, with the Chowla–Selberg form [65]

$$P_{\mathrm{num}} = \Gamma(\tfrac{1}{15})\,\Gamma(\tfrac{2}{15})\,\Gamma(\tfrac{4}{15})\,\Gamma(\tfrac{8}{15}), \qquad L(f_3,2) = \frac{P_{\mathrm{num}}}{120\sqrt{3}\,\pi}\,, \tag{59}$$

which an independent evaluation confirms to 70 digits. The identity (59) is known; here we obtain it using only the Picard–Fuchs operator and its Frobenius traces. The quasi-period and L-value constructions lift to the equal-mass three-loop banana: an Eichler-integral representation fixed in the same way reproduces its quasi-period block to 159 digits, and the two critical L-values of its newform f_3 are Chowla–Selberg monomials, matched to 70 digits. A degree-one period-polynomial bootstrap was attempted at this rung and did not pass, for lack of the exact multiplier system of the level-15 form; the failure is multiplier-system-limited, not precision-limited.

The complete equal-mass banana integrals have simpler boundary constants: at three loops the ε^0 constant of the top master is a rational multiple of ζ_3 [59], and at four loops those of all

five masters across $\varepsilon^{-4}\dots\varepsilon^{0}$ lie in the ζ-ring [13, 58]. The CM period of Eq. (59) can enter the three-loop integral only at higher orders in ε, where its identification is still pending (a raw-master normalization reconciliation). For the boundary values of the ice-cream cone (Sec. 6) we have found no analogous ring.

6 The ice-cream cone

We compute the two-loop ice-cream cone graph, whose Landau singularities were analyzed by Hannesdottir, McLeod, Schwartz and Vergu [41] (Sec. 6.4 of that work), in $d = 2 - 2\varepsilon$ dimensions on a one-scale slice, at equal internal masses and at one point with four distinct masses. The maximal cut of its sunrise subgraph is an elliptic curve, non-modular at generic masses, and the graph has a Landau singularity of its own.

6.1 Kinematics and the integral family

We label the four internal lines $q_1, \dots, q_4$, with masses $m_1, \dots, m_4$, and the six external legs $p_1, \dots, p_6$. Momentum conservation reads

$$p_1 + p_2 = q_2 + q_3 + q_4, \qquad p_4 - p_3 = -q_1 + q_3 + q_4, \qquad p_5 + p_6 = q_1 + q_2, \tag{60}$$

with invariants $p_{12}^2 = (p_1 + p_2)^2$, $p_{34}^2 = (p_3 - p_4)^2$ and $p_{56}^2 = (p_5 + p_6)^2$. We work on the symmetric one-scale slice

$$p_{12}^2 = p_{34}^2 = x, \qquad p_{56}^2 = -1, \qquad d = 2 - 2\varepsilon, \tag{61}$$

in units of m_1^2, for two mass configurations: equal masses, $m_j^2 = 1$, and the single all-distinct mass point $m^2 = (1, 2, 3, 5)$. We fix boundary values at $x = -1$ and evaluate the integral at any Euclidean point $x < -\frac{1}{2}$ of that slice.

In terms of the loop momenta ℓ_1, ℓ_2 and the combinations $P_{12} = p_1 + p_2$, $P_{56} = p_5 + p_6$ and $P_{34} = p_4 - p_3 = P_{12} - P_{56}$, the propagators are

$$D_1 = \ell_2^2 - m_1^2, \quad D_2 = (P_{56} - \ell_2)^2 - m_2^2, \quad D_3 = \ell_1^2 - m_3^2, \quad D_4 = (P_{12} - P_{56} + \ell_2 - \ell_1)^2 - m_4^2, \tag{62}$$

with the scalar products $D_5 = (\ell_1 + P_{56})^2$, $D_6 = (\ell_2 + P_{12})^2$, $D_7 = (\ell_1 + P_{12})^2$ completing the basis. We compute the scalar member $[1, 1, 1, 1, 0, 0, 0]$ of this family,

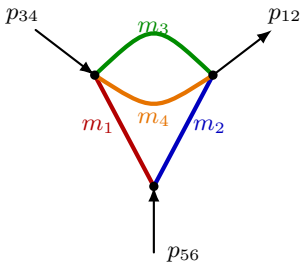

$$= \; I_{\mathrm{ICC}}(x) = \int \frac{\mathrm{d}^d\ell_1\, \mathrm{d}^d\ell_2}{(i\pi^{d/2})^2} \frac{1}{D_1 D_2 D_3 D_4}, \qquad d = 2 - 2\varepsilon. \tag{63}$$

In the graph, colors mark the masses. The sub-sectors are the sunrise subgraph $[1, 0, 1, 1]$ on lines $1, 3, 4$ (masses $(1, 3, 5)$ at the generic point), a second sunrise $[0, 1, 1, 1]$ on lines $2, 3, 4$ (masses $(2, 3, 5)$; at equal mass the two coincide), and the bubble $[1, 1, 0, 0]$. Reducing by integration by parts with Kira [46], we find 7 master integrals at equal mass (5 of uniform transcendental weight) and 19 at the generic mass point.

In Feynman parameters,

$$I_{\mathrm{ICC}} \propto \int_0^\infty \Big(\prod_{e=1}^{4} \mathrm{d}x_e\Big)\, \delta\Big(1-\textstyle\sum_e x_e\Big)\, \frac{\mathcal{U}^{\nu-(L+1)d/2}}{\mathcal{F}^{\nu-Ld/2}}, \qquad L=2,\ \nu=4, \tag{64}$$

with the Symanzik polynomials

$$\mathcal{U} = x_1x_2+x_1x_3+x_1x_4+x_2x_3+x_2x_4, \qquad \mathcal{F}\big|_{m_e=0} = p_1^2\, x_1x_2x_4 + p_2^2\, x_1x_2x_3 + p_3^2\,(x_1x_3x_4+x_2x_3x_4), \tag{65}$$

and $\mathcal{F} = \mathcal{F}|_{m_e=0} + \mathcal{U}\cdot(\sum_e m_e^2 x_e)$. Here x_1, x_2 are the parameters of D_3, D_4 and x_3, x_4 those of D_1, D_2 (m_e is the mass on the line of parameter x_e), $p_3^2 = p_{56}^2$, and $\{p_1^2, p_2^2\} = \{p_{12}^2, p_{34}^2\}$, both equal to x on the slice. The mass term is quadratic in the individual x_e, which makes the maximal cut of the sunrise subgraph a curve of genus one.

The integral (63) is ultraviolet and infrared finite (its superficial degree of divergence is $\omega = Ld - 2\cdot 4 = -4-4\varepsilon < 0$ and all internal lines are massive), and its ε-expansion starts at ε^0. We follow the $d_0 = 2$ convention of the sunrise literature [4] because in two dimensions the maximal cut of the sunrise subgraph is directly the holomorphic period of the curve (66). Since Tarasov's dimension shift to $d = 4$ involves the higher orders in ε, we also compute the order ε^1.

6.2 Maximal-cut curves and periods

In $d = 2$ the maximal cut of the sunrise subgraph, taken loop by loop, is the one-dimensional integral $\oint \mathrm{d}s/Y$ over the invariant mass squared s of the pair (D_3, D_4), where

$$Y^2 = \lambda(s, m_3^2, m_4^2)\, \lambda(s, m_1^2, x) \tag{66}$$

and λ is the Källén function. The four branch points $s = (m_3 \pm m_4)^2$ and $s = (\sqrt{x} \pm m_1)^2$ of this elliptic curve collide in pairs at $x = 0$ and at $x = (\pm m_1 \pm m_3 \pm m_4)^2$. At the generic mass point we thus find the singular locus $x\, Q_{\mathrm{sc}}(x)$, with

$$Q_{\mathrm{sc}}(x) = x^4 - 36x^3 + 302x^2 - 564x + 121 = \prod_{\pm} (x - (\pm 1 \pm \sqrt{3} \pm \sqrt{5})^2), \tag{67}$$

the product over the normal threshold and the three pseudo-thresholds of the $(1, 3, 5)$ sunrise [2]. This curve is non-modular; its monodromy is not a congruence subgroup, so no $\Gamma_1(N)$ uniformization exists. Similarly, the second sunrise (masses $(2, 3, 5)$) defines a distinct curve, with

$$Q_{14}(x) = x^4 - 40x^3 + 352x^2 - 960x + 576 = \prod_{\pm} (x - (\sqrt{2} \pm \sqrt{3} \pm \sqrt{5})^2), \tag{68}$$

the subscript being the label of its sector (masters $11, \ldots, 14$ of the 19-master basis).

We denote by ψ_1, ψ_2 two solutions of the Picard–Fuchs equation of the curve (66). At the generic mass point it reads

$$\psi'' + P_1(x)\, \psi' + P_0(x)\, \psi = 0, \tag{69}$$

with

$$\begin{aligned} P_1 &= \frac{1}{\Delta}\big(24x^9 - 996x^8 + 15584x^7 - 113796x^6 + 369775x^5 \\ &\qquad - 346709x^4 - 60058x^3 + 170738x^2 + 50435x - 9317\big), \\ P_0 &= \frac{1}{\Delta}\big(24x^7 + 442x^6 - 8170x^5 + 32705x^4 - 18952x^3 + 6992x^2 + 15106x + 6237\big), \\ \Delta &= x\,(2x+1)\,(2x^2 - 17x - 7)\,(3x^2 - 18x + 11)\, Q_{\mathrm{sc}}(x). \end{aligned} \tag{70}$$

The genuine singular points are the zeros of $x\,Q_{\rm sc}(x)$; the other factors of Δ contribute only apparent singularities (at the zeros of $3x^2-18x+11$ the local exponents are $\{0,2\}$). We take ψ_1 to be the holomorphic period and fix the second solution by $(\psi_2,\psi_2')\big|_{-1}=(0,1)$.

At equal mass the curve (66) becomes $Y^2=s(s-4)\,\lambda(s,1,x)$, the equal-mass sunrise curve [12, 4] with monodromy group $\Gamma_1(6)$, cusps $\{0,1,9,\infty\}$ and singular locus $x(x-1)(x-9)$. The sunrise master S (the sub-sector integral $[1,0,1,1]$ at $d=2$) obeys the inhomogeneous equation [52]

$$S''+p_1S'+p_0S=\frac{6}{x(x-1)(x-9)},\qquad p_1=\frac{3x^2-20x+9}{D},\quad p_0=\frac{x-3}{D},\quad D=x(x-1)(x-9), \tag{71}$$

whose homogeneous solutions are the equal-mass sunrise period ψ_1 and a second solution ψ_2, again fixed by $(\psi_2,\psi_2')\big|_{-1}=(0,1)$. Since the $\Gamma_1(6)$ curve is modular, it has a ring of cusp constants (zeta values and logarithms) in which we can look for boundary values; the generic curve (67) has no such ring.

6.3 Landau singularities and the alphabet

We obtain the singular locus of the family with the programs `PLD.jl` [35] and `SOFIA.jl` [26], in agreement with refs. [41, 10]. At equal mass m the leading Landau locus of the cone, with all four Feynman parameters nonzero (eq. (6.48) of ref. [41]), is

$$L_{\rm icc}=p_{12}^2p_{34}^2p_{56}^2+m^2\big[\,9m^2p_{56}^2+(p_{12}^2-p_{34}^2)^2-5(p_{12}^2+p_{34}^2)p_{56}^2+4p_{56}^4\,\big]=0. \tag{72}$$

On the slice $p_{12}^2=p_{34}^2=x$, $p_{56}^2=w$, $m^2=1$ this locus and the second-type (Källén) locus of the underlying triangle graph reduce to

$$L_{\rm icc}\big|_{\rm slice}=w\,(x^2-10x+4w+9),\qquad L_{\delta}\big|_{\rm slice}=w\,(w-4x), \tag{73}$$

and at $w=-1$ the first becomes

$$L_{\rm bub}=x^2-10x+5=(x-r_+)(x-r_-),\qquad r_\pm=5\pm2\sqrt{5}=\{9.4721\ldots,\,0.5279\ldots\}. \tag{74}$$

With the sunrise points and two removable letters, the equal-mass alphabet is

$$\{\,x,\;x-1,\;x-9,\;2x+1,\;4x+1,\;L_{\rm bub}\,\}. \tag{75}$$

Physically, $x=0$ is the first-entry letter of the p_{12}^2 channel, and $x=1$, $x=9$ are the pseudo-threshold and the normal threshold $(3m)^2$ of the sunrise subgraph, both cusps of $\Gamma_1(6)$. At $x=r_\pm$ the pair (D_3,D_4) sits at its threshold on the locus (72) (equivalently, $L_{\rm bub}$ is the Landau locus of the triangle with masses $(m,m,2m)$), and $2x+1$, $4x+1$ come from the external Gram determinants and are removable (Fig. 3).

At the generic mass point we find in place of the quadratic (74) the quartic

$$L_{\rm bub}=x^4-40x^3+348x^2-880x+196\quad\text{(irreducible over }\mathbb{Q}), \tag{76}$$

which is eq. (6.48) of ref. [41] with all four $\alpha_e\neq0$ and, up to the factor 4, the product of the threshold and pseudo-threshold Landau loci of the triangle $(m_1,m_2,m_3\pm m_4)$. The letter $L_{\rm bub}$ is confined to the top sector. Dividing every denominator of the 19×19 connection matrix of Sec. 6.4 by it, we find $L_{\rm bub}$ only in the top-sector rows $\{15,16,17,18\}$ and not in the rows $\{5,6,7,8\}$ and $\{11,12,13,14\}$ of the two sunrises. At equal mass the poles at $x=r_\pm$ likewise sit only in the top rows $(4,5,6)$, with diagonal residue $A[4][4]\big|_{r_+}=-\frac{4}{11}-\frac{6\sqrt{5}}{55}$, and not in the rows $(2,3)$. The letter $L_{\rm bub}$ already appears in the integration-by-parts reduction: the coefficient of the top integral in the reduction of its dotted partner is $((2-d)x+d-3)/(x^2-10x+5)$.

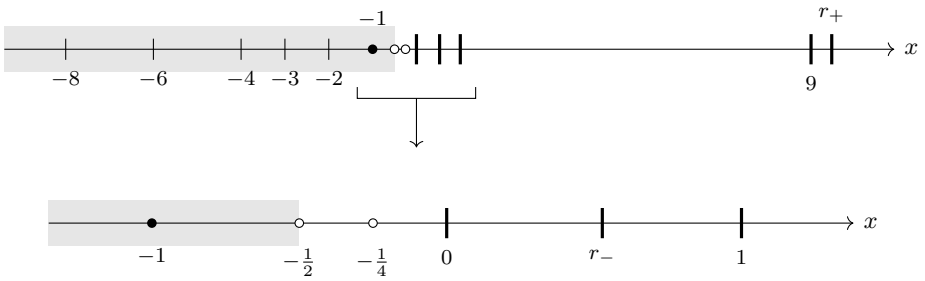

Figure 3: The alphabet of the equal-mass ice-cream cone on the real x-line, the boundary point $x = -1$ where the constants are fixed, and the Euclidean points at which the closed form is compared with numerical evaluations (Table 2 and App. C.1). Thick bars mark the letters of Eq. (75) that are singular points of the solution: the sunrise points $x = 0, 1, 9$ and the roots $r_\pm = 5 \pm 2\sqrt{5}$ of the cone's own letter $L_{\rm bub}$; open circles mark the apparent singular points $x = -\frac{1}{2}, -\frac{1}{4}$ of the differential equation; the filled dot is the boundary point; short ticks are the comparison points $x = -2, -3, -4, -6, -8$; the shaded half-line $x < -\frac{1}{2}$ is the region in which we evaluate the closed form. Both axes are to scale; the lower one magnifies the neighborhood of the origin.

6.4 The differential equation

The vector M of master integrals obeys

$$\partial_x M = A(d, x)\, M, \qquad A(2 - 2\varepsilon, x) = \sum_{k \geq 0} \varepsilon^k A^{(k)}(x), \tag{77}$$

with A rational in x and d and block-lower-triangular by sector; this system is not in the ε-form of Eq. (1). We expand the masters as $M_j = \sum_k \varepsilon^k f_{j,k}(x)$. The top integral (63) has index $j = 4$ at equal mass (15 at the generic point) and the sunrise master $j = 2$ (5); we abbreviate $T \equiv f_{4,0}$ and $S \equiv f_{2,0}$ (or $f_{15,0}$, $f_{5,0}$). We derive A from a Baikov representation or, equivalently, from differential operators in the external invariants. Order by order in ε we solve each diagonal block of Eq. (77) by variation of parameters over its homogeneous solutions, through which the periods enter. The lower blocks form the source, and every $f_{j,k}$ is then an iterated integral of the class of Eq. (11).

At the generic mass point we find for the self-coupling of the top and its coupling c_S to the sunrise subgraph

$$A[15][15] = \frac{-270x^4 + 2706x^3 - 8658x^2 + 10676x - 4004}{(4x+1)\,(x^4 - 40x^3 + 348x^2 - 880x + 196)}, \tag{78}$$

$$c_S(x) = \frac{\begin{aligned}&-192x^9 + 8550x^8 - 118439x^7 + 691024x^6 - 1762968x^5\\ &+ 1499645x^4 + 880795x^3 - 1000411x^2 - 61114x + 58410\end{aligned}}{(2x+1)(4x+1)\,(x^4 - 40x^3 + 348x^2 - 880x + 196)\,(x^4 - 36x^3 + 302x^2 - 564x + 121)}, \tag{79}$$

the latter with both $L_{\rm bub}$ and $Q_{\rm sc}$ in its denominator. The self-coupling of the sunrise subgraph and its source from the bubble sector read

$$A[5][5] = \frac{10x^4 - 121x^3 + 336x^2 + 27x - 24}{(2x+1)\,Q_{\rm sc}(x)}, \qquad A[5][4] = \frac{-3x^4 + 78x^3 - 350x^2 + 94x + 77}{(2x+1)\,Q_{\rm sc}(x)}. \tag{80}$$

At equal mass the coupling of the sunrise subgraph to the top is

$$c_S(x) = A[4][2] = \frac{2\,(10x^4 - 65x^3 - 131x^2 + 37x + 45)}{3\,(x-9)(x-1)(2x+1)(4x+1)\,(x^2 - 10x + 5)}, \tag{81}$$

with a simple pole at $L_{\rm bub} = 0$.

As shown in refs. [50, 28], the top sector of the cone in $d = 2$ has a rank-two differential operator with algebraic (Liouvillian) solutions for generic masses and momenta. The third-order operator of ref. [27] for the top integral factorizes accordingly into a first-order and a second-order factor. Consequently the sunrise periods enter the top integral only through its source, and the top integral can be obtained by variation of parameters over an algebraic kernel. In our basis, at equal mass and at order ε^0 (grade zero), the top sector closes on T and the dotted top (master 5 of that basis). Eliminating the latter, we obtain

$$\begin{aligned} L_T &= \partial_x^2 + \tilde{p}_1\,\partial_x + \tilde{p}_0, \qquad \tilde{p}_1 = \frac{14x^5 - 155x^4 + 520x^3 - 316x^2 + 22x - 5}{(x-1)(4x+1)(x^2-10x+5)(x^2-4x+1)}, \\ \tilde{p}_0 &= \frac{6\,(x^4 - 8x^3 + 24x^2 - 4x + 3)}{(x-1)(4x+1)(x^2-10x+5)(x^2-4x+1)}, \end{aligned} \tag{82}$$

whose kernel is algebraic,

$$\begin{aligned} y_\pm(x) &= q_\pm(x)^{-1/2}, \qquad q_\pm = \tfrac{1}{2}\Big(2x^2 + 8x - 5 \pm \sqrt{5}\,(2x-1)\sqrt{4x+1}\Big), \\ q_+ q_- &= (x-1)^2\,(x^2 - 10x + 5), \end{aligned} \tag{83}$$

with local exponents $\{-\frac{1}{2}, 0\}$ at $r_\pm$, $\{0, \frac{1}{2}\}$ at $x = -\frac{1}{4}$ and $\{0, 2\}$ at $x = 2 \pm \sqrt{3}$.

We thus arrive at the inhomogeneous equation for the top,

$$L_T[T] = \alpha(x)\,S(x) + \beta(x)\,S'(x) + g_1(x) - g_t(x)\,\mathrm{Tri}_0, \tag{84}$$

with

$$\begin{aligned} \alpha &= \frac{-8\,(2x^4 - 9x^3 - 15x^2 - 25x - 15)}{3(x-9)(x-1)(4x+1)(x^2-10x+5)(x^2-4x+1)}, \\ \beta &= \frac{-2\,(11x^5 - 63x^4 + 48x^3 - 340x^2 + 165x - 45)}{3(x-9)(x-1)(4x+1)(x^2-10x+5)(x^2-4x+1)}, \\ g_1 &= \frac{8}{(x-9)(x-1)(x^2-10x+5)}, \qquad g_t = \frac{2\,(2x^3 - 27x^2 + 18x - 1)}{(x-1)(4x+1)(x^2-10x+5)(x^2-4x+1)}. \end{aligned} \tag{85}$$

Here $\mathrm{Tri}_0 = 4\ln\varphi/\sqrt{5}$, with φ the golden ratio, is the $d = 2$ bubble of the lines D_1, D_2 at $p_{56}^2 = -1$, and the terms $g_1 - g_t\,\mathrm{Tri}_0$ are the contribution of the bubble and tadpole masters. At the generic mass point the source is the sum of a rational function, a rational function times S (through c_S of Eq. (79)) and a rational function times S_{14}, the period of the second sunrise. This period enters the source through the entries $A[15][11], \ldots, A[15][14]$, which have Q_{14} of Eq. (68) in their denominators. However, for generic masses and momenta the homogeneous top block is the rank-two algebraic operator of refs. [50, 28], which we have not reduced our 19-master system to (our grade-zero elimination there is third-order).

6.5 Boundary conditions and the closed form

With $L_{\rm PF}$ the operator on the left of Eq. (71), the sunrise master at equal mass is

$$S = A\,\psi_1 + B\,\psi_2 + 6P, \qquad L_{\rm PF}[S] = \frac{6}{x(x-1)(x-9)}, \tag{86}$$

with source constant 6, where P is the particular solution with unit source,

$$L_{\rm PF}[P] = \frac{1}{x(x-1)(x-9)}, \qquad (P, P')\big|_{-1} = (0,0). \tag{87}$$

Since $\psi_2(-1) = P(-1) = 0$, we read off the two constants from the value and the derivative of S at the boundary point, after continuing S there from its large-x cusp expansion, whose free coefficients are logarithmic in the masses and vanish at equal mass: $A = S(-1)/\psi_1(-1) = -2.4880163\ldots$ and $B = S'(-1) - A\,\psi_1'(-1) = +0.33712992\ldots$ (Table 2). The bubble and tadpole masters are elementary; their Laurent coefficients ($-2\gamma_E$ and $2\gamma_E^2 + \pi^2/6$ at orders ε^{-1} and ε^0 for the divergent bubble-sector master, the integers $(1, -2, 1)$ at order ε^{-2} for the tadpoles) enter the top only through g_1 and g_t.

We now write the top integral at equal mass in closed form by variation of parameters over the algebraic pair (83):

$$\boxed{T(x) = c_+ y_+(x) + c_- y_-(x) + \int_{-1}^{x} \frac{y_-(x)\,y_+(x') - y_+(x)\,y_-(x')}{W(x')}\,(\alpha S + \beta S' + g_1 - g_t \mathrm{Tri}_0)(x')\,\mathrm{d}x'} \tag{88}$$

with $W = y_+ y_-' - y_+' y_-$ the Wronskian, α, β, g_1, g_t the kernels of Eq. (85), and two constants $c_\pm$. For Euclidean $x < -\frac{1}{4}$ the $y_\pm$ are complex conjugates, and so are $c_\pm$. Equation (88) is the main result of this section. It is an iterated integral of transcendental weight three in the class (11), a single integral of algebraic kernels against a source containing the period pair of the curve (66), with the six letters of Eq. (75). Its singular points are the sunrise cusps $x = 0, 1, 9$ (through the source), the apparent points $x = -\frac{1}{2}, -\frac{1}{4}$, and the branch points $r_\pm$ of $L_{\rm bub}$, where L_T has exponents $\{-\frac{1}{2}, 0\}$. Because the period pair ψ_1, ψ_2 enters the integrand, $T(x)$ is not a multiple polylogarithm.

We derive $c_\pm$ from two conditions at the large-x cusp. In $u = 1/x$ the operator L_T has indicial exponents $\{1, \frac{3}{2}\}$ at $u = 0$, and the general solution of Eq. (84) behaves there as

$$T = u\,(t_{11}\ln(-u) + t_{10}) + C\,u^{3/2}(1 + O(u)) + \ldots, \qquad u = \frac{1}{x}, \tag{89}$$

the omitted terms being fixed by the source once t_{10} and C are given. First we set $C = 0$, because the large-x expansion of a Feynman integral contains only integer powers of u times logarithms. Second, we fix t_{10} by matching to the large-x region in which the pair (D_3, D_4) carries the large momentum (hard-bubble matching); the resulting constant τ_0 is proportional to $\ln(m_3^2 m_4^2)\,\mathrm{Tri}_0$ and vanishes at equal mass, $t_{10} = \tau_0 = 0$. The logarithmic coefficient requires no further input, since the resonance of the exponent 1 with the source forces $t_{11} = 2\,\mathrm{Tri}_0 = 8\ln\varphi/\sqrt{5}$, which is also the value obtained from the hard region. Continuing the solution so determined from the cusp to $x = -1$, we obtain $T(-1)$ and $T'(-1)$, hence $c_\pm$. In this way the two cusp conditions give, with no numerical input anywhere in the chain, the boundary value

$$T(-1) = 0.60984239\ldots, \tag{90}$$

in agreement with an `AMFlow` [53] evaluation to 199 of its 202 digits (Table 2).

We have searched for a closed form of $T(-1)$ with the PSLQ algorithm. At 120 digits, a search in the weight-three ring

$$\{1, \pi^2, \zeta_3, \pi^2\log 2, \pi^2\log 3, \log^3 2, \log^3 3, \psi, \psi\pi^2, \psi^3, \psi\log^2 2, \pi^2/\psi, \psi^2, \psi^2\pi\}, \qquad \psi \equiv \psi_1(-1), \quad (91)$$

with integer coefficients up to 10^9 returns only a dense seven-digit-coefficient relation, which is spurious and rejected. For the ratio $T(-1)/\psi_1(-1)$ in the classical ring $\{1, \pi, \pi^2, \log 2, \log 3, \log^2 2, \sqrt{5}, \sqrt{3}, \zeta_3, \pi^2\log 2\}$ with coefficients up to 10^8 we find no relation. The constant $T(-1)$ is thus an elliptic period of transcendental weight three lying, like A and B, outside the classical cusp ring at the searched heights, which is a search result and not a theorem.

6.6 The boundary value as a period

The boundary value $T(-1)$ has a direct integral representation. Feynman-combining the pair (D_3, D_4) gives one line of spectral mass squared $s(a) = m_3^2/a + m_4^2/(1-a)$, raised to the power $2 - d/2$, and the remaining loop is a one-loop triangle with internal masses $(m_1^2, m_2^2, s(a))$. To all orders in ε,

$$T(\varepsilon; x) \;=\; \Gamma(2+2\varepsilon) \int_0^1 \mathrm{d}a \int_\Delta \mathrm{d}^2\alpha \, \left[a(1-a)\right]^{-1-\varepsilon} \alpha_3^{\varepsilon} \, F(\alpha; s(a); x)^{-2-2\varepsilon}, \quad (92)$$

where $T(\varepsilon; x) = \sum_k \varepsilon^k f_{4,k}(x)$, Δ is the simplex $\alpha_1 + \alpha_2 + \alpha_3 = 1$ with α_3 the parameter of the spectral line, and F is the second Symanzik polynomial of the triangle on the slice,

$$F(\alpha; s; x) = \alpha_1 m_1^2 + \alpha_2 m_2^2 + \alpha_3\, s - w\, \alpha_1\alpha_2 - x\, \alpha_3(\alpha_1 + \alpha_2), \qquad w = p_{56}^2 = -1. \quad (93)$$

At orders ε^0 and ε^1 we can do one of the two integrals over α in terms of logarithms and dilogarithms, which leaves a convergent two-fold integral.

At equal mass the Landau locus of the effective triangle is the pair of zeros

$$s_\pm(x) = \tfrac{1}{2}(3 + 2x \pm \sqrt{5}\sqrt{4x+1}) \quad (94)$$

of its Cayley determinant $2(s+1-x)^2 - 10s$, and at the threshold $s = (m_3 + m_4)^2$ of the spectral line this determinant vanishes precisely on $L_{\mathrm{bub}} = 0$. In $d = 2$ this triangle reduces to its three bubbles, and at order ε^0 and equal mass we can collapse Eq. (92) to the one-fold integral

$$\begin{aligned} T(x) &= 2\int_4^\infty \frac{\mathrm{d}s}{\sqrt{s(s-4)}} \, \frac{2(c-2s)\, B(s;x) + (2c-5)\,\mathrm{Tri}_0}{2c^2 - 10s}, \qquad c = s + 1 - x, \\ B(s;x) &= \int_0^1 \frac{\mathrm{d}a}{a + s(1-a) - x\, a(1-a)}, \end{aligned} \quad (95)$$

with B the $d = 2$ bubble of masses squared $(1, s)$ at momentum squared x. The Tri_0 term integrates in closed form through its residues at $s_\pm$. The remainder is the integral of the bubble logarithm against $\mathrm{d}s/Y$ on the curve $Y^2 = s(s-4)\,\lambda(s, 1, x)$, with simple poles at $s_\pm$, i.e. a length-two elliptic polylogarithm with two third-kind punctures. Evaluating Eq. (92) by direct quadrature, we reproduce the boundary value (90) to 284 digits (Table 2).

6.7 The generic mass point

At the mass point $m^2 = (1, 2, 3, 5)$ most of the construction goes through unchanged. The curve (66) with singular locus $x\, Q_{\mathrm{sc}}(x)$, the alphabet with the letter L_{bub} of Eq. (76) confined to the top rows,

the 19×19 connection matrix with the kernels (78)–(80), and the structure of the source described in Sec. 6.4 are all known analytically. In the lower sectors the sunrise master is $S = \psi_1 E_0$, with E_0 a combination of elliptic dilogarithms on the $(1, 3, 5)$ curve given in ref. [64], and the period S_{14} of the second sunrise solves its own second-order equation. At large x we impose the same two conditions as at equal mass, now with a nonzero hard-bubble constant

$$\tau_0 = \ln 15 \cdot \ln(1 + \sqrt{2})/\sqrt{2} \tag{96}$$

from $m_3^2 m_4^2 = 15$, where $\ln(1 + \sqrt{2})/\sqrt{2}$ is the value of Tri_0 for the masses $(m_1^2, m_2^2) = (1, 2)$.

We lack an analog of the algebraic homogeneous pair (83) for the generic-mass top block, which we have not brought to rank-two form (Sec. 6.4). Without a closed form like Eq. (88), we therefore integrate the system (77) numerically from $x = -1$ (App. C.1). We derive the boundary vector at $x = -1$ in App. B.3, independently of `AMFlow`; its top component is defined by the integral (92) with $m^2 = (1, 2, 3, 5)$. The boundary value of the top, and two values of the solution, are

$$\begin{aligned} T(-1) &= 0.13489705\ldots, \\ T(-2) &= 0.13100788\ldots, \\ T(-3) &= 0.12736077\ldots, \end{aligned} \tag{97}$$

in agreement with numerical evaluations (Table 2). In contrast with the equal-mass case, here the $(1, 3, 5)$ curve is non-modular and there is no ring of cusp constants; the fiber at $x = -1$ has $j = 470596/225$, not an algebraic integer, so it has no complex multiplication either, and ψ_1 is itself transported rather than known in closed form (we obtain $\psi_1(-1)$ by numerical solution of Eq. (69)). Searches for $T(-1)$ against the period lattice of the curve and against the L-value and regulator ring of $\mathbb{Q}(\sqrt{3}, \sqrt{5})$, to height 10^{12}, find no relation [64].

6.8 Order ε

At order ε^1 and equal mass the top row of Eq. (77) gives

$$\frac{\mathrm{d}}{\mathrm{d}x} f_{4,1} = A^{(0)}_{4j} f_{j,1} + A^{(1)}_{4j} f_{j,0} + A^{(2)}_{4j} f_{j,-1} + \cdots, \tag{98}$$

summed over j. We list the rational kernels $A^{(k)}_{4j}$ in App. B.1; L_{bub} divides their denominators at both orders, and $A^{(0)}_{4,2}$ is the coupling c_S of Eq. (81), through which the period ψ_1 enters the weight-four top integral $f_{4,1}$ as well. Eliminating the dotted top as before, we find for $f_{4,1}$ an inhomogeneous equation with the operator L_T of Eq. (82) and a grade-one source. In this source the masters $f_{j,0}$ (the top pair included) enter through $A^{(1)}$ and the sub-sector masters $f_{j,1}$ through $A^{(0)}$. We obtain $f_{4,1}$ by one further integration against the same algebraic kernel, as a length-three iterated integral with one new boundary constant

$$f_{4,1}(-1) = -0.67751873\ldots \tag{99}$$

At 110 digits an integer-relation search for this constant in the weight-four ring

$$\{1, \pi^2, \zeta_3, L, L^2, L^3, \pi^2 L, \psi, \psi\pi^2, \psi L^2, \psi^2, 1/\psi, \pi^2/\psi\}, \qquad \psi \equiv \psi_1(-1), \quad L \equiv \log|q(-1)|, \tag{100}$$

with q the nome of the $\Gamma_1(6)$ curve and coefficients up to 10^6, finds no relation, and we have not identified this constant.

The inputs to the two cusp conditions at this order are nevertheless in closed form. They include the next two Laurent coefficients of the bubble master at $p_{56}^2 = -1$,

$$c_{1,0} = 2\gamma_E \,\mathrm{Tri}_0 + J, \qquad c_{1,1} = -\Big((2\gamma_E^2 + \zeta_2)\,\mathrm{Tri}_0 + 2\gamma_E J + \tfrac{K}{2}\Big),$$
$$J = \int_0^1 \frac{\ln(1+a-a^2)}{1+a-a^2}\,\mathrm{d}a, \qquad K = \int_0^1 \frac{\ln^2(1+a-a^2)}{1+a-a^2}\,\mathrm{d}a. \tag{101}$$

The coefficients (101) lie in the ring of logarithms and dilogarithms of the golden ratio. The order-ε^1 cusp constants of the sunrise subgraph, $(-\pi^2, -18\zeta_3)$, follow from Mellin residues of its d-dimensional Bessel representation, and the two cusp conditions with these inputs reproduce the value (99) to 127 digits (Table 2).

6.9 Sequential discontinuities

The ice-cream cone is the example by which ref. [41] established a violation of the strict hierarchical principle [51, 17]. The strict form confines the singularities of an absorption integral to higher-order leading singularities, with all Feynman parameters of the inserted graph nonzero; the weak (Pham) form also admits branches of a dominating graph's Pham locus on which some parameters vanish. In the slice variables of Eq. (73) the principal subleading loci are the normal threshold of the sunrise subgraph, $x = (3m)^2 = 9$, and the bubble, $w = (2m)^2 = 4$. In particular, the bubble-like singularity of ref. [41] (their eq. (4.4), with $\alpha_3 = \alpha_4 = 0$ and $\alpha_1, \alpha_2 \neq 0$) obeys the same Landau equations as the bubble and sits on the same locus, $p_{56}^2 = (m_1 + m_2)^2$. The slice $w = -1$ misses this locus; it crosses the cone's own Pham locus only on the leading component L_{bub}, where the zeros $s_\pm(x)$ of Eq. (94) reach the threshold $s = 4$ of the pair (D_3, D_4), with all parameters nonzero.

The letter L_{bub} enters the differential equation (77) only in the top rows and the closed form (88) only through the branch points $r_\pm$ of the kernels $y_\pm$, where L_T has local exponents $\{-\frac{1}{2}, 0\}$. On the slice the singularity at $L_{\mathrm{bub}} = 0$ is thus present in the top integral and absent from every subsector, as the Landau equations require. The sequential discontinuity that contradicts the strict principle, $(1-\mathcal{M}_{\mathrm{bub}})(1-\mathcal{M}_{\mathrm{icc}})I_{\mathrm{ICC}} \neq 0$ with $\mathcal{M}_{\mathrm{bub}}$ the monodromy around the bubble-like branch at $p_{56}^2 = (m_1+m_2)^2$ (eqs. (6.62)–(6.63) of ref. [41]), lives off this slice, which therefore cannot exhibit it. The sequential discontinuities in the orders sunrise-then-bubble and bubble-then-sunrise vanish by the compatibility argument of Sec. 7 of ref. [41]. Exhibiting the nonvanishing discontinuity would require a two-scale slice through $p_{56}^2 = (m_1 + m_2)^2$, which we have not computed.

6.10 Numerical comparisons

Finally, we compare the closed forms and boundary values with numerical evaluations. For the cone these are auxiliary-mass-flow [53] values of the master integrals: the Laurent expansions at $x = -1$, and values at Euclidean points $x = -2, -3, \ldots$ that enter no step of the construction. We evaluate the closed form (88), its order-ε^1 analog and the generic-mass solution by series solution of the ε-expanded system (77) from $x = -1$ (App. C.1), and Eq. (92) by direct quadrature. The closed form and the generic-mass solution agree with these values to 135 and 108 digits at $x = -2$ and to 75 and 68 at ε^1; Table 2 lists all comparisons. At the generic mass point the order-ε^0 solution also agrees to 88 digits, at $x = -2$ and $x = -3$, with values sampled independently before the differential-equation solution existed.

An alternative to integrating the differential equation of the top would be a fit of its sampled values to a basis of iterated integrals over the sunrise kernels. Empirically, at equal mass, the blind canonical-frame fit floors at 15 digits, while a fit of the sunrise-subgraph master from the same data

quantity	configuration, point	compared with	digits	note
(a) Threshold coefficients and L-values, Secs. 3–5				
$c_{3/4}$, $c_{5/4}$, Eq. (43)	sunrise $(1,1,4)$	PF continuation	159	ball arithmetic
$c_{3/2}$, Eq. (38)	banana $(1,1,1,9)$	PF continuation	195	ball arithmetic
$c_{5/4}$, $c_{7/4}$, Eq. (41)	banana $(1^4,16)$	PF continuation	197	ball radii 198 and 197; integer relations of height 4 and 15, stable at 118 and 197 working digits
$c_{3/2}$, Eq. (45)	CY_4 slice $(1^5,25)$	PF continuation	248	ball arithmetic
$A_1 = \frac{3}{2}\,c_{3/2}$, Eq. (46)	banana $(1,1,1,9)$	PF continuation	77	evaluation not used in any fit
A_0, Eq. (46)	banana $(1,1,1,9)$	PF continuation	153	ball arithmetic
A_0 moment identity, Eq. (49)	banana $(1,1,1,9)$	direct integration	34	
α_1 as a Bessel moment	banana $(1^4,16)$	direct integration	35	
α_1, α_2, Eq. (51)	banana $(1^4,16)$	two continuations	101	
E_2 quasi-period, Eq. (57)	sunrise, equal mass	PF continuation	99	five Euclidean points, worst case
$L(f_3,2)$ from Frobenius traces	sunrise $(1,1,4)$	newform L-value	55	integer-relation precision
$L(f_3,2)$, Eq. (59)	Γ-product	newform L-value	70	no free constant
K3 quasi-period block	banana, equal mass	PF continuation	159	six points; distinct from the first row
K3 critical L-values	banana, equal mass	eta-quotient	70	
(b) The ice-cream cone, Sec. 6				
$T(-1)$, Eq. (90)	equal mass, $x=-1$	`AMFlow`	199	of a 202-digit value; derived boundary
$T(x)$, Eq. (88)	equal mass, $x=-2$	`AMFlow`	134	135 in a second run at higher working precision
$T(x)$ at order ε^0	$m^2=(1,2,3,5)$, $x=-2$	`AMFlow`	118	against a 210-digit value
$T(x)$ at order ε^0	$m^2=(1,2,3,5)$, $x=-2,-3$	earlier `AMFlow` values	88	sampled before the solution existed
$T(-1)$, Eq. (97)	$m^2=(1,2,3,5)$, $x=-1$	`AMFlow`	133	of a 210-digit value; derived boundary vector
$f_{4,1}(x)$ at order ε^1	equal mass, $x=-2$	`AMFlow`	134	75 by the series solution at the truncation order of App. C.1
top at order ε^1	$m^2=(1,2,3,5)$, $x=-2,-3$	`AMFlow`	68	
Eq. (92) by quadrature	equal mass, $x=-1$	`AMFlow`	284	of a 330-digit value
Eq. (95)	equal mass, $x=-1$	`AMFlow`	330	working precision 345
Eq. (95), generic analog	$m^2=(1,2,3,5)$, $x=-1$	`AMFlow`	209	of a 210-digit value; working precision 230
Eq. (92) at order ε^1	equal mass, $x=-1$	`AMFlow`	133	
cusp conditions for $f_{4,1}(-1)$	equal mass, $x=-1$	`AMFlow`	127	inputs of Eq. (101)
S, Eq. (86)	equal mass, $x=-2,-3,\ldots$	`AMFlow`	61–62	62 at $x=-3$, 61 at the worst point
$S=\psi_1 E_0$	$m^2=(1,2,3,5)$	`AMFlow`	60	

Table 2: Agreement, in digits, between the closed forms and boundary values of this paper and numerical evaluations not used in their derivation. Block (a): the threshold coefficients of Secs. 3–4 at the coalescence point $t=0$ and the quasi-periods and L-values of Sec. 5, against numerical continuation of the Picard–Fuchs operators ("PF continuation"), direct integration of the stated Bessel moments, or the L-values of the newforms; block (b): the ice-cream cone of Sec. 6 against auxiliary-mass-flow evaluations [53]. Digit counts are rounded down; "ball arithmetic" marks entries with rigorous error radii; working precisions and reference lengths are stated where they limit the count (App. C). Mass labels list the squared masses, with $(1^4,16)\equiv(1,1,1,1,16)$ and $(1^5,25)\equiv(1,1,1,1,1,25)$.

reaches 89–91 digits. The particular solution of the top, an integral of S and S' against algebraic kernels, lies outside the span of such a basis, which is why we integrate the differential equation from the boundary value (90). Appendix C gives working precisions, truncation orders and the search settings.

7 Conclusions

In this paper we studied sunrise and banana integrals whose heaviest internal mass equals the sum of the others. We showed that the sunrise elliptic surface has an additive fiber of Kodaira Type III at the coalescence point $t = 0$, with local monodromy of order four, and is therefore not modular. At three loops the local monodromy there consists of a rank-three unipotent block and the order-two factor known from the equal-mass K3 surface [13, 23], whereas for generic masses that monodromy is unipotent. Through five loops the order of the finite monodromy factor alternates between four and two (Table 1), depending on whether the inverse powers in the non-oscillatory Bessel tail are half-integral or integral. From that tail we derived the connection coefficients in closed form: rational multiples of $\sqrt{3}/\pi$ at three loops and, up to a power of $\sqrt{2}$, elements of the lemniscatic ring (13) at two and four loops. Neither the equal-mass nor the three-equal-mass three-loop banana can realize a non-CM weight-3 period (Proposition 5.1).

We also treated one complete integral, the two-loop ice-cream cone in $d = 2 - 2\varepsilon$ dimensions. At equal mass its order-ε^0 top integral is a single integral of algebraic kernels against the period pair of the sunrise subgraph, with the boundary constants fixed at the large-momentum cusp. Its one new constant is the elliptic period $T(-1)$. At one generic mass point we again obtained the kernels and the boundary vector, and the top block is integrated numerically.

The Type III fiber, the indicial polynomials (Table 1), the connection coefficients (Sec. 4) and the equal-mass closed form (Sec. 6) are exact. Proposition 5.1 is a corollary of the factorization of refs. [32, 31], the lattice classification of ref. [30] and Livné's theorem [54]. The Bessel-moment identity for A_0 and the vanishing of one logarithmic coefficient at four loops (Sec. 4.3) are numerical statements, as is the analyticity of the complete two-, three- and four-loop integrals at the coalescence point (Sec. 3.4). At three loops we infer the order of the finite monodromy factor from the period monodromy only (App. A), and no five-loop graph realizing the last row of Table 1 is known. All closed forms were compared with independent numerical evaluations (Table 2, App. C).

It would be interesting to know which other graphs acquire additive fibers at threshold configurations, and of which Kodaira types. In particular, we have not found a graph realizing the Type II pencil of App. A. In the pairwise-equal banana or on a surface with a nebentypus character, a non-CM weight-3 period could still arise (Sec. 5). The arithmetic nature of the boundary period $T(-1)$ is open. We have not examined how an ε-form for the unequal-mass bananas continues through a point of finite local monodromy. We expect the Picard–Fuchs operator and, where available, the Bessel representation to determine the local structure at threshold configurations of other Calabi–Yau families.

Acknowledgments

Funding for this project was provided by Anthropic. This is not an official Anthropic project and results and views are not endorsed by Anthropic.

A Threshold fibers and operators

We collect here the Weierstrass models and Picard–Fuchs operators used in Sec. 3, and the evidence for the geometric label of Sec. 3.2.

A.1 The Type III fiber

We write the cut quartic of Eq. (15) as $P(y;t) = a\,y^4 + b\,y^3 + c\,y^2 + d\,y + e$, with coefficients polynomial in t and in the squared masses. Its classical invariants are

$$I = 12ae - 3bd + c^2, \qquad J = 72ace + 9bcd - 27ad^2 - 27eb^2 - 2c^3, \tag{102}$$

and the Jacobian of the curve $Y^2 = P(y;t)$ is the (I,J)-Jacobian model

$$\eta^2 = \xi^3 + A(t)\,\xi + B(t), \qquad A = -27\,I, \qquad B = -27\,J, \tag{103}$$

with $c_4 = -48A$, $c_6 = -864B$ and $\Delta = -16\,(4A^3 + 27B^2)$. At $(M_1, M_2, M_3) = (1, 1, 4)$ this gives the coefficients of Eq. (17), with discriminant $\Delta(t) = 8707129344\,t^3(t-16)^2(t-4)^4$. Both A and B vanish at $t = 0$. This is the additive condition, and j stays finite there ($j(0) = 1728$, with $v_{t=0}(j - 1728) = 1$). Running Tate's algorithm at $t = 0$ we find: $v(\Delta) = 3 > 0$; the singular point of the reduced curve has $v(b_2) = \infty$, hence the fiber is additive; $v(a_6) = 2$ is not smaller than 2, which excludes Type II; and $v(b_8) = 2 < 3$, which gives Type III [49]. The other singular fibers are I_4 at $t = 4$, I_2 at $t = 16$ and I_3 at $t = \infty$, Eq. (18); the conductor exponent at $t = 0$ is $f = 2$, and the Euler numbers of the four singular fibers add up to $3 + 4 + 2 + 3 = 12$. The curve $Y^2 = P(y;t)$ has a rational point at infinity (the coefficient of y^4 is 1), and Nagell's reduction with respect to it gives a second model of the same curve,

$$\begin{aligned}\eta^2 = \xi^3 &+ (4t^2 + 192)\,\xi^2 + (128t^3 - 256t^2 - 4096t + 12288)\,\xi \\ &+ (1024t^4 - 16384t^3 + 98304t^2 - 262144t + 262144)\,,\end{aligned} \tag{104}$$

with the same j-invariant as a function of t. Running Tate's algorithm on Eq. (104) we obtain the same configuration $[\mathrm{III}, I_4, I_2, I_3]$. These two applications of Tate's algorithm, a computer-algebra run of it on the model (103), and the local exponents $\pm\frac{1}{4}$ of the operator (20) are the four identifications of Table 3.

The parity argument of Sec. 3.1, which excludes Type II fibers from the family (15), runs as follows. An additive fiber of the family needs a triple root of $P(y;0) = \lambda(y, M_1, M_2)\,(y - M_3)^2$, hence $\lambda(M_3, M_1, M_2) = 0$. On both branches $\sqrt{M_3} = \sqrt{M_1} \pm \sqrt{M_2}$ of that locus, for generic M_1 and M_2, we find $(v_{t=0}(c_4), v_{t=0}(c_6), v_{t=0}(\Delta)) = (1, 2, 3)$ for the model (103). In particular, $v(c_6) = 2$ is even at every additive fiber of the family, whereas Type II has $(v(c_4), v(c_6), v(\Delta)) = (\geq 1, 1, 2)$ and $j \to 0$ [49]. A Type II fiber requires the three colliding Weierstrass roots to lie in one ramified orbit, $\xi_k - \xi_* \sim \zeta_3^k (t - t_*)^{1/3}$, hence an irreducible cubic. It does occur on the pencil

$$\eta^2 = \xi^3 + (t-1)\,\xi + (t-1)\,, \tag{105}$$

which has $\Delta = -16\,(t-1)^2(4t+23)$ and $j(t) = 6912\,(1-t)/(-4t-23)$; its fiber at $t = 1$ has $(v(c_4), v(c_6), v(\Delta)) = (1, 1, 2)$ and $j(1) = 0$. A by-hand Tate branching, which exits at $v(a_6) = 1 < 2$, and two computer-algebra reductions (the PARI functions `ellfromeqn` and `elllocalred`) all give Type II there. We expect pencils of this kind to arise from elliptic sub-sectors whose Baikov cut is an irreducible, non-Källén cubic. Which named graph and mass tuple realize that pencil remains open, and the additive-fiber gallery beyond these two entries is deferred.

Route	Method	Result
(i)	Picard–Fuchs / Griffiths–Dwork; indicial $r = \pm\frac{1}{4}$ at t=0	order-4 monodromy, eigenvalues $\pm i$
(ii)	Tate's algorithm on the (I, J)-Jacobian model	Type III, f=2, Euler sum 12
(iii)	Independent Nagell Weierstrass model (distinct polynomial form)	same config [III, I_4, I_2, I_3]
(iv)	By-hand Tate branching ($v(b_8)$=2<3 ⇒ Type III)	Type III; no table lookup

Table 3: Four identifications of the fiber at $t = 0$ for the $(1, 1, 4)$ sunrise agree on Kodaira Type III. Route (i) uses the Picard–Fuchs operator (20) of the period on the model (103), without Tate's algorithm; routes (ii) and (iii) are computer-algebra runs of Tate's algorithm on the polynomially distinct Weierstrass models (17) and (104); in route (iv) we follow the branching of the algorithm by hand. For the two-mass family $(1, 1, M)$, with M the third squared mass, the fiber at $t = 0$ is multiplicative of Type I_1 whenever $M \neq 4$, including at the equal-mass point (the $\Gamma_1(6)$ surface); the fiber type therefore changes only at the threshold configuration $M = 4$.

A.2 Picard–Fuchs operators

The sunrise operator (20), obtained by Griffiths–Dwork reduction on the model (103) for the period $\Pi(t) = \oint \mathrm{d}\xi/\eta$, has singular points $t \in \{0, 4, 16, \infty\}$ and local exponents

$$\{-\tfrac{1}{4}, \tfrac{1}{4}\} \text{ at } t = 0, \qquad \{0, 0\} \text{ at } t = 4 \text{ and at } t = 16, \qquad \{1, 1\} \text{ at } t = \infty\,. \tag{106}$$

For the banana family we use the variable $z = -1/t$, which puts the point of maximal unipotent monodromy at $z = 0$ and the coalescence point at $z = \infty$, and the derivation $\theta = z\,\mathrm{d}/\mathrm{d}z$. Near $z = 0$ we normalize the holomorphic period of the L-loop banana with squared masses $M_1, \ldots, M_{L+1}$ as the series [14]

$$\varpi_0 = \sum_{n\geq 0} c_n\,(-z)^n, \qquad c_n = \sum_{k_1+\cdots+k_{L+1}=n} \binom{n}{k_1, \ldots, k_{L+1}}^2 \prod_{i=1}^{L+1} M_i^{k_i}\,, \tag{107}$$

and each operator below, $\mathcal{L} = \sum_j P_j(z)\,\theta^j$ with integer coefficients, annihilates it term by term. If d is the common degree of the P_j, a local solution $t^\rho(1 + O(t))$ at the coalescence point has ρ a root of $\sum_j([z^d]P_j)(-\rho)^j$. We write indicial polynomials in the variable r of Table 1; there and in Sec. 3 they are quoted up to normalization. We obtain each operator from the series (107) by the following search. For trial values of the order and of d we solve $\mathcal{L}\varpi_0 = 0$ for the coefficients of the P_j modulo 31-bit primes, keep the smallest order and then the smallest d with a solution, and reconstruct the rational coefficients by Chinese remaindering over eight primes. The reconstructed operator then annihilates the exact series term by term beyond the coefficients used in the fit: $n = 87$–118 for Eq. (108), at least 130 coefficients for Eq. (110), and 361 coefficients for Eq. (109) (reconstructed over sixteen primes). Each operator is minimal in the sense that this search finds no annihilator of lower order, or of the same order and lower degree.

Three loops, $(M_i) = (1,1,1,9)$, order four and $d = 5$, with coefficients

$$\begin{aligned}
P_4 &= 36864\,z^5 + 63232\,z^4 + 20448\,z^3 + 2032\,z^2 + 78\,z + 1\,,\\
P_3 &= 165888\,z^5 + 303872\,z^4 + 66272\,z^3 + 3704\,z^2 + 40\,z - 1\,,\\
P_2 &= 276480\,z^5 + 563008\,z^4 + 87880\,z^3 + 4156\,z^2 + 54\,z\,,\\
P_1 &= 202752\,z^5 + 458304\,z^4 + 55464\,z^3 + 2424\,z^2 + 12\,z\,,\\
P_0 &= 55296\,z^5 + 137088\,z^4 + 13968\,z^3 + 576\,z^2\,.
\end{aligned} \tag{108}$$

The indicial polynomial at the coalescence point is $18432\,(r-1)^3(2r-3)$, Eq. (23), and at $z = 0$ it is $r^3(r-1)$; the leading coefficient is $P_4 = (4z+1)(16z+1)(36z+1)(16z^2+22z+1)$, with zeros at $t = 4, 16, 36$ and at the roots of $t^2 - 22t + 16$.

Three loops, generic point $(1,1,4,9)$, order five and $d = 11$, with coefficients

$$\begin{aligned}
P_5 &= 5682318075\,z^{11} + 17598088998\,z^{10} + 20014381251\,z^9 + 10040176276\,z^8\\
&\quad + 1956538422\,z^7 - 60785644\,z^6 - 91575074\,z^5 - 17393552\,z^4\\
&\quad - 1660497\,z^3 - 86058\,z^2 - 2177\,z - 20\,,\\
P_4 &= 51140862675\,z^{11} + 130240419939\,z^{10} + 118819214820\,z^9 + 44408552840\,z^8\\
&\quad + 3048386666\,z^7 - 2231037078\,z^6 - 672783364\,z^5 - 88012540\,z^4\\
&\quad - 5921445\,z^3 - 163221\,z^2 + 648\,z + 60\,,\\
P_3 &= 176151860325\,z^{11} + 384587371602\,z^{10} + 290492367399\,z^9 + 77570474648\,z^8\\
&\quad - 6038647302\,z^7 - 7492033772\,z^6 - 1655851210\,z^5 - 185353312\,z^4\\
&\quad - 10402671\,z^3 - 201846\,z^2 + 179\,z - 40\,,\\
P_2 &= 289798221825\,z^{11} + 563255181027\,z^{10} + 361766166732\,z^9 + 62166922966\,z^8\\
&\quad - 20605309220\,z^7 - 11007304212\,z^6 - 2070411686\,z^5 - 210585158\,z^4\\
&\quad - 9888669\,z^3 - 108255\,z^2 + 1050\,z\,,\\
P_1 &= 227292723000\,z^{11} + 405719482014\,z^{10} + 227249430822\,z^9 + 20335504434\,z^8\\
&\quad - 19684521030\,z^7 - 7677470610\,z^6 - 1297419642\,z^5 - 122353866\,z^4\\
&\quad - 4893642\,z^3 - 24180\,z^2 + 300\,z\,,\\
P_0 &= 68187816900\,z^{11} + 114409341648\,z^{10} + 57170797920\,z^9 + 1128899412\,z^8\\
&\quad - 6387680052\,z^7 - 2089125864\,z^6 - 326459448\,z^5 - 28787580\,z^4\\
&\quad - 998136\,z^3\,.
\end{aligned} \tag{109}$$

The indicial polynomial at $t = 0$ is $-5682318075\,(r-3)(r-2)^2(r-1)^2$, whose roots are the integer exponents $\{1,1,2,2,3\}$ quoted in Sec. 3.2, and at $z = 0$ it is $-20\,r^3(r-2)(r-1)$; P_5 contains the factors $(z+1)^2(9z+1)^2(25z+1)(49z+1)$, with zeros at the singular points $t = 1, 9, 25, 49$. The exponents quoted in Table 1 must be read off from minimal operators, because a non-minimal annihilator has additional local exponents, determined by its extra left factor, and these can be fractional. We hit this failure mode ourselves: the order-six operator we first obtained at $(1,1,4,9)$ was later found to be non-minimal, with true minimal order five and z-degree eleven as in Eq. (109). Writing $\mathcal{L}_6$ for the order-six operator and $\mathcal{L}_5$ for the operator (109), we find an exact division $\mathcal{L}_6 = Q\,\mathcal{L}_5$; the non-integer indicial exponents of $\mathcal{L}_6$ belong to the left factor Q and do not occur in the indicial polynomial of $\mathcal{L}_5$. At the second coalescence $(1,4,4,9)$ of Sec. 3.2 the minimal operator likewise has order five and z-degree eleven; it annihilates the series exactly over 370 terms, and its indicial polynomial at $t = 0$ is $(r-2)(r-1)^3(2r-3)$.

Four loops, $(M_i) = (1,1,1,1,16)$, order six and $d = 9$, with coefficients

$$
\begin{aligned}
P_6 &= 48922361856\,z^9 - 6370099200\,z^8 + 11541086208\,z^7 + 6748073984\,z^6 \\
&\quad + 839681280\,z^5 + 46303296\,z^4 + 1360432\,z^3 + 18396\,z^2 \\
&\quad + 24\,z - 1\,, \\
P_5 &= 440301256704\,z^9 - 150759014400\,z^8 + 154779844608\,z^7 + 54403985408\,z^6 \\
&\quad + 4263832320\,z^5 + 147633024\,z^4 + 1990960\,z^3 - 30864\,z^2 \\
&\quad - 672\,z + 2\,, \\
P_4 &= 1623610884096\,z^9 - 765898260480\,z^8 + 787866845184\,z^7 + 175548016640\,z^6 \\
&\quad + 10208241984\,z^5 + 338424912\,z^4 + 3920536\,z^3 - 41892\,z^2 \\
&\quad + 180\,z - 1\,, \\
P_3 &= 3137146454016\,z^9 - 1730118942720\,z^8 + 1929830989824\,z^7 + 297808437248\,z^6 \\
&\quad + 14887650688\,z^5 + 460978016\,z^4 + 1237040\,z^3 - 84368\,z^2 \\
&\quad - 112\,z\,, \\
P_2 &= 3348124139520\,z^9 - 2011464990720\,z^8 + 2472912027648\,z^7 + 286440962048\,z^6 \\
&\quad + 13287063360\,z^5 + 379326928\,z^4 - 1036024\,z^3 - 60768\,z^2 \\
&\quad - 20\,z\,, \\
P_1 &= 1871280340992\,z^9 - 1180591718400\,z^8 + 1599509495808\,z^7 + 148504248320\,z^6 \\
&\quad + 6636381440\,z^5 + 174709056\,z^4 - 1403872\,z^3 - 22240\,z^2\,, \\
P_0 &= 428070666240\,z^9 - 277736325120\,z^8 + 412251586560\,z^7 + 32313384960\,z^6 \\
&\quad + 1420765440\,z^5 + 34367040\,z^4 - 449760\,z^3 - 3360\,z^2\,.
\end{aligned}
\tag{110}
$$

The indicial polynomial at the coalescence point is $3057647616\,(r-2)^2(r-1)^2(4r-7)(4r-5)$, Eq. (28), and at $z = 0$ it is $-r^4(r-1)^2$; P_6 contains the factor $(4z+1)(16z+1)(36z+1)(64z+1)$. Similarly, at the generic point $(1,1,1,1,9)$ we find a minimal operator with the same $(\text{order}, d) = (6,9)$ and integer exponents $\{1,1,2,2,3,3\}$ at $t = 0$.

Five loops, the slice $(M_i) = (1,1,1,1,1,25)$ of Sec. 3.3, order eight and $d = 14$, with coefficients

$$
\begin{aligned}
P_8 &= 1262682245714411520000\, z^{14} - 162978756058467532800\, z^{13} - 440882373674171105280\, z^{12} \\
&\quad - 91347632004150591488\, z^{11} - 866351410810454016\, z^{10} + 630596191411503104\, z^9 \\
&\quad + 44966204165308416\, z^8 + 1543224351768576\, z^7 + 29437804680192\, z^6 \\
&\quad + 119374792704\, z^5 - 6752313024\, z^4 - 115320192\, z^3 \\
&\quad - 517712\, z^2 + 96\, z - 1\,, \\
P_7 &= 19571574808573378560000\, z^{14} - 5692272592489021440000\, z^{13} - 677363570970017660928 0\, z^{12} \\
&\quad - 843341232668154003456\, z^{11} + 55894216663924867072\, z^{10} + 8269823864642961408\, z^9 \\
&\quad + 324698831066333184\, z^8 + 6907114504753152\, z^7 + 21842155083264\, z^6 \\
&\quad - 3433981047936\, z^5 - 63340634304\, z^4 - 66715584\, z^3 \\
&\quad + 2827656\, z^2 - 1814\, z + 3\,, \\
P_6 &= 130056271308584386560000\, z^{14} - 52584372821543406796800\, z^{13} - 44117712555601444208640\, z^{12} \\
&\quad - 271927733541974468198 4\, z^{11} + 519065099117717815296\, z^{10} + 3744844765997403340 8\, z^9 \\
&\quad + 1141200321847885824\, z^8 + 23001165288044544\, z^7 - 118162367890176\, z^6 \\
&\quad - 13298910687744\, z^5 - 96122298432\, z^4 + 343074720\, z^3 \\
&\quad - 5189604\, z^2 + 696\, z - 3\,, \\
P_5 &= 483607300108619612160000\, z^{14} - 2346146049195836964864 00\, z^{13} - 162793838102621989109760\, z^{12} \\
&\quad - 163756456646132839219 2\, z^{11} + 2024901960210866536448\, z^{10} + 976708452279025745 92\, z^9 \\
&\quad + 2867793891930961920\, z^8 + 43687149219165696\, z^7 - 1027931520749568\, z^6 \\
&\quad - 35914588152192\, z^5 - 153208043040\, z^4 + 2188776\, z^3 \\
&\quad + 1593144\, z^2 - 508\, z + 1\,, \\
P_4 &= 1099796236017252433920000\, z^{14} - 5978807843825733599232 00\, z^{13} - 372780128332139326341120\, z^{12} \\
&\quad + 123735500008751848488 96\, z^{11} + 4440430219422666096640\, z^{10} + 167295805865730760704\, z^9 \\
&\quad + 4826883535953586176\, z^8 + 48630323825644032\, z^7 - 2513508017332992\, z^6 \\
&\quad - 56119985443200\, z^5 - 72499292832\, z^4 - 8864904\, z^3 \\
&\quad - 1372764\, z^2 - 200\, z\,, \\
P_3 &= 1565094643563013079040000\, z^{14} - 9181517558683671724032 00\, z^{13} - 539854285730119837286400\, z^{12} \\
&\quad + 374173129079716986224 64\, z^{11} + 5925846008968358559744\, z^{10} + 193112649272054489088\, z^9 \\
&\quad + 5397641740327778304\, z^8 + 30393937146809856\, z^7 - 3745758789898752\, z^6 \\
&\quad - 55660387944192\, z^5 - 1869180384\, z^4 - 269831544\, z^3 \\
&\quad - 1020576\, z^2 - 30\, z\,, \\
P_2 &= 1359908778634421207040000\, z^{14} - 8414058306986047438848 00\, z^{13} - 480165486890736785817600\, z^{12} \\
&\quad + 477015876056506664222 72\, z^{11} + 4806237246767640510464\, z^{10} + 145153653565680197632\, z^9 \\
&\quad + 3821347973427574784\, z^8 + 5986928299818496\, z^7 - 3323489471618560\, z^6 \\
&\quad - 33856531640960\, z^5 + 19896564512\, z^4 - 260988344\, z^3 \\
&\quad - 472016\, z^2\,, \\
P_1 &= 6591201322629228134400 00\, z^{14} - 4237706655547879587840 00\, z^{13} - 238737323761662217420800\, z^{12} \\
&\quad + 296758008557499501772 80\, z^{11} + 2185935854696519761920\, z^{10} + 64027398414562181120\, z^9 \\
&\quad + 1544435398792048640\, z^8 - 3457628835732480\, z^7 - 1638655605570560\, z^6 \\
&\quad - 11386785224960\, z^5 + 8774091840\, z^4 - 114424720\, z^3 \\
&\quad - 126880\, z^2\,, \\
P_0 &= 1363696825371564441600 00\, z^{14} - 9019533227644787097600 0\, z^{13} - 506548731519524929536 00\, z^{12} \\
&\quad + 734931053586119393280 0\, z^{11} + 428240585230067957760\, z^{10} + 12511583454886625280\, z^9 \\
&\quad + 270988445081763840\, z^8 - 1626133209477120\, z^7 - 345052030771200\, z^6 \\
&\quad - 1599203573760\, z^5 + 918397440\, z^4 - 20777280\, z^3 \\
&\quad - 15360\, z^2\,.
\end{aligned}
\tag{111}
$$

The indicial polynomial at the coalescence point is $631341122857205760000\,(r-3)^2(r-2)^3(r-1)^2(2r-3)$, Table 1, and at $z=0$ it is $-r^5(r-1)^3$; P_8 contains the factor $(4z+1)(16z+1)(36z+1)(64z+1)(100z+1)$. On the generic slice $(1,1,1,1,1,30)$ we find $(\text{order}, d) = (8, 16)$ and integer exponents $\{1,1,2,2,3,3,4,4\}$ at $t=0$.

A.3 Evidence for the K3 label

At $(1,1,1,9)$ the indicial polynomial of Eq. (108) and the Frobenius branch (24), whose expansion coefficients lie in $\mathbb{Q}$, are exact and fix the local monodromy spectrum $\{1,1,1,-1\}$ at $t=0$. Integrating Eq. (108) numerically around $t=0$, using none of the indicial data, we recover the eigenvalue -1 to $\sim 10^{-12}$. The geometric label of Sec. 3.2, a non-semistable degeneration of the K3 family in which the finite part of the local monodromy has order two, rests on weaker evidence. In the loop-by-loop Baikov representation the maximal cut is a double cover of the plane branched along three conics (the iterated Källén factors), fibered by genus-one curves. Tate's algorithm on the Jacobian of the fiber, with the discriminant computed from the fiber quartic, gives at $(1,1,1,9)$ an additive fiber of Type III at $t=0$ with $(v_{t=0}(c_4), v_{t=0}(c_6), v_{t=0}(\Delta)) = (1,2,3)$ and $j = 1728$. At the generic point $(1,1,4,9)$ the same computation gives $v_{t=0}(\Delta) = 1$ and $j=\infty$ (Type I_1), and at $(1,4,4,9)$ Type III again. A Picard–Lefschetz analysis of the vanishing cycles on the same model is consistent with the spectrum $\{1,1,1,-1\}$.

We also tried two further computations, both inconclusive. The first, a computation of the local monodromy after the base change $t=\tau^2$, gave the identity, as it does for a multiplicative I_1 fiber, whose monodromy is unipotent; this test is therefore blind to the unipotent part. The second, a direct numerical integration of the reduced period around $t=0$, gave a non-symplectic matrix. Of the evidence above, therefore, only the period monodromy of Eq. (108), through its exact indicial data and the numerically recovered eigenvalue, supports the statement that the finite part of the local monodromy at the coalescence point has order two. The Tate and Picard–Lefschetz computations on the Baikov model are consistent with this order.

One earlier analysis of ours reached the opposite conclusion: classifying the local singularities of the Baikov branch sextic (nodes, ordinary triple points, tacnodes), we found no tacnode at the coalescence point of $(1,1,1,9)$ and concluded that the local monodromy there is unipotent. However, the singularity type of the branch curve does not determine the period monodromy at $t=0$, whereas the numerical integration of Eq. (108) gives the eigenvalue -1 of that monodromy directly. The tacnode that the earlier analysis does detect lies on the mass-equality locus (the Shioda–Inose product K3); it is present at all t and is unrelated to the threshold coalescence.

B Further formulas for the ice-cream cone

In this appendix we collect details omitted from Sec. 6: the order-ε kernels of the top row, the Feynman-parameter form of the boundary integral, and the construction of the boundary vector at the generic mass point.

B.1 Order-ε kernels and cusp data

At equal mass the order-ε coefficient $f_{4,1}$ of the top master obeys Eq. (98), whose kernels $A_{4j}^{(k)}$ are the coefficients of ε^k in row 4 of the connection matrix at $d = 2-2\varepsilon$; below we write $A_{4,j}^{(\varepsilon^k)} \equiv A_{4j}^{(k)}$. Rows $4,5,6$ belong to the top sector, and column 2 multiplies the sunrise-subgraph master $S \equiv f_{2,0}$.

Columns 0 and 1 multiply the two x-independent masters

$$f_0 = \varepsilon^{-2}\,\Gamma(1+\varepsilon)^2\,, \qquad f_1 = -\Gamma(\varepsilon)\,\Gamma(1+\varepsilon)\int_0^1 (1+a-a^2)^{-1-\varepsilon}\,\mathrm{d}a\,, \tag{112}$$

where the Laurent expansion of f_0 gives the bubble-sector constants of Sec. 6.5 and that of f_1 the cusp data of Sec. 6.8, namely $c_{1,-1} = -\mathrm{Tri}_0$ and the coefficients $c_{1,0}$, $c_{1,1}$ of Eq. (101). The row-4 entries that enter are

$$\begin{aligned}
A_{4,4}^{(\varepsilon^0)} &= \frac{2(-3x^3+19x^2-5x-3)}{(x-1)(4x+1)(x^2-10x+5)}, & A_{4,4}^{(\varepsilon^1)} &= \frac{2(-2x^3+8x^2+x-2)}{(x-1)(4x+1)(x^2-10x+5)},\\
A_{4,5}^{(\varepsilon^0)} &= \frac{2(x^2-4x+1)}{(x-1)(4x+1)(x^2-10x+5)}, & A_{4,5}^{(\varepsilon^1)} &= \frac{2(-9x^2-10x+7)}{(x-1)(4x+1)(x^2-10x+5)},\\
A_{4,6}^{(\varepsilon^1)} &= \frac{6(3x-2)}{(x-1)(4x+1)(x^2-10x+5)}, & A_{4,1}^{(\varepsilon^1)} &= \frac{2x}{(x-1)(x^2-10x+5)},
\end{aligned} \tag{113}$$

and the order-ε^0 couplings to S and f_0,

$$\begin{aligned}
A_{4,2}^{(\varepsilon^0)} &= \frac{2(10x^4-65x^3-131x^2+37x+45)}{3(x-9)(x-1)(2x+1)(4x+1)(x^2-10x+5)},\\
A_{4,0}^{(\varepsilon^0)} &= \frac{4x^2(4x^2-3x-1)}{(x-9)(x-1)(2x+1)(4x+1)(x^2-10x+5)}.
\end{aligned} \tag{114}$$

Here $A_{4,2}^{(\varepsilon^0)}$ is the coupling c_S of Eq. (81), and $L_{\mathrm{bub}} = x^2-10x+5$ divides every denominator.

B.2 Ingredients of the boundary integral

In the coordinates $\alpha_1 = ut$, $\alpha_2 = u(1-t)$, $\alpha_3 = 1-u$ (with $\mathrm{d}^2\alpha = u\,\mathrm{d}u\,\mathrm{d}t$ on the unit square) the polynomial F of Eq. (93) at $w=-1$ is quadratic in u,

$$F = s + \left[m_2^2 - s - x + (m_1^2 - m_2^2)\,t\right]u + (x + t - t^2)\,u^2\,. \tag{115}$$

For Euclidean $x < -\frac{1}{4}$ the coefficient of u^2 is negative and $F > 0$ on the closed unit square. Expanding Eq. (92) in ε, we obtain for the first two coefficients of $T(\varepsilon;x) = \sum_k \varepsilon^k f_{4,k}(x)$

$$T(x) = \int_0^1 \frac{\mathrm{d}a}{a(1-a)}\int_0^1 \mathrm{d}t\int_0^1 \frac{u\,\mathrm{d}u}{F^2}\,, \tag{116}$$

$$f_{4,1}(x) = 2(1-\gamma_E)\,T(x) + \int_0^1 \frac{\mathrm{d}a}{a(1-a)}\int_0^1 \mathrm{d}t\int_0^1 \frac{u\,\mathrm{d}u}{F^2}\Big[\ln(1-u) - 2\ln F - \ln\big(a(1-a)\big)\Big], \tag{117}$$

with F taken at $s = s(a)$. The u-integral is elementary (a rational function of the roots of Eq. (115) in u plus a logarithm at order ε^0 and dilogarithms at order ε), which leaves a convergent integral over (a,t). At equal mass we substitute $s = 1/(a(1-a))$ on each half of the a-interval, which gives $\mathrm{d}a/(a(1-a)) = \mathrm{d}s/\sqrt{s(s-4)}$ with $s \geq 4$. Reducing the $d=2$ triangle to its bubbles, we then obtain Eq. (95) from Eq. (116).

B.3 The generic-mass boundary vector

Solving the system (77) numerically at $m^2 = (1,2,3,5)$ requires at $x=-1$ the Laurent coefficients of all masters through order ε^0. For the series solution of App. C.1 we take them from `AMFlow`;

here we derive the same boundary vector independently, as follows. The tadpole and bubble subsectors are elementary, as at equal mass, and the sunrise masters S and S_{14} are evaluated at the boundary point from their own integral representations. The two sunrise sub-blocks (the sunrise-sector masters other than S and S_{14}) and the top sector contribute 25 further coefficients to the boundary vector. Seven of them, at order ε^{-2}, are exact rationals, and eight, at order ε^{-1}, are elementary closed forms.

At order ε^0 the coefficients of the two sunrise sub-blocks and of the top sector are fixed at the large-x cusp and continued numerically to $x = -1$. Six follow from four resonance conditions. At a resonant cusp exponent the Frobenius recursion leaves a coefficient of the local expansion undetermined, and we fix it, as for τ_0 in Sec. 6.7, by matching the large-x behavior of the sub-block masters. We obtain two more by solving the cusp recursions of two top-sector components as a coupled system. The last two, $T(-1)$ of Eq. (97) among them, follow from the cusp conditions on the top sector, and $T(-1)$ is also given directly by the integral (92). No generic boundary coefficient is fabricated. The coefficients so obtained agree with independent `AMFlow` [53] evaluations to at least 109 digits (the full length of the reference values) for twenty-three of the twenty-five, and to at least 89 digits for all 25 at a lower working precision.

C Numerical methods and integer-relation searches

Digit counts quoted in this paper are recorded agreements, rounded down, never working precisions, except where a sentence labels a number as a working precision or as an internal consistency depth. In this appendix we give the settings of the series solutions, numerical continuations and integer-relation searches behind these counts, and the comparisons with `AMFlow` not listed in Table 2.

C.1 Series solutions and comparisons

We evaluate the ice-cream cone of Sec. 6 away from $x = -1$ by series solution of its differential equation expanded in ε. With $M_j(x) = \sum_K f_{j,K}(x)\,\varepsilon^K$ for each master integral and $A(2-2\varepsilon, x) = \sum_{k\geq 0} A^{(k)}(x)\,\varepsilon^k$ for the connection matrix, the system $\partial_x M = A\,M$ reads

$$f'_{i,K}(x) = \sum_{j,\,k\geq 0} A^{(k)}_{ij}(x)\, f_{j,\,K-k}(x), \tag{118}$$

which we integrate from $x = -1$ by local Taylor series whose radius is set by the nearest singular points of A, at $x = -1/4, -1/2$. At equal mass we use order 60 at a working precision of 130 digits for the 14-component state. In the generic-mass slice we use order 45 at 90 digits for the 57-component state (19 masters $\times$ orders $\varepsilon^{-2}, \varepsilon^{-1}, \varepsilon^0$). The initial data are the ε-Laurent expansions of all masters at $x = -1$. We compute them by the auxiliary-mass-flow method [53] with Kira [46] reductions, to $\sim$ 120 digits at equal mass and $\sim$ 111 digits in the generic slice. We evaluate the sunrise period ψ_1 that enters the source term to 769 digits. For the order-ε^0 comparisons at $x = -2$ in Table 2 whose digit counts exceed the working precisions of these series solutions, we made separate runs of the same method at higher Taylor order and working precision. Of these runs, the equal-mass one started from the boundary values of Sec. 6.5 instead of the `AMFlow` expansions.

We also compare the series solutions with `AMFlow` at Euclidean points beyond those of Table 2. At equal mass and order ε^0, with Taylor order 44 at working precision 130 we find agreement to 70, 69, 68, 68 digits at $x = -3, -4, -6, -8$. With order 60 and the same boundary data the agreement is 95, 94, 93, 93 digits, while the `AMFlow` uncertainties there allow at least 110 digits, so the printed floors are truncation-limited, not reference-limited. At order ε^1 we find agreement at equal mass to

74, 74, 75 digits at $x = -3, -5/2, -4$, and a solution restarted from $x = -4$ reproduces the values at $x = -2, -3$ to 70 digits. The weight-four cusp data of Eq. (101) differ from the series solution by $\leq 5 \times 10^{-51}$.

C.2 The threshold coefficients

For the numerical continuations of Sec. 4.1 we expand ϖ_0 at the point of maximal unipotent monodromy, continue it to a circle around the coalescence point and apply the projector of Eq. (30). For the four-loop coefficients of Eq. (41) we ran two continuations that share only the operator (order 6, z-degree 9; App. A.2). The first works in s in multiple-precision floating point and takes the expansion coefficients of ϖ_0 from their closed multinomial formula (107). The second works in $z = -1/s$ in Arb [45] ball arithmetic at 896 bits, generates the same coefficients from the recurrence implied by the operator, and follows a different monodromy contour. The coefficients obtained in the two ways agree over 301 terms.

In ball arithmetic we obtain rigorous enclosures of the four-loop coefficients $c_{5/4}$ and $c_{7/4}$ to 198 and 197 digits. Their midpoints agree with Eq. (41) to 260/259 digits and are independent of the matching radius to 260/258 digits; these are midpoint comparisons, corroborative rather than ball-certified. The floating-point continuation reproduces both coefficients to 72/71 digits, the limit of its working precision. Substituting the three-loop operator, we recover the K3 coefficient $c_{3/2} = -\sqrt{3}/(36\pi)$ in the same two continuations, to 223 digits in ball arithmetic (a midpoint comparison; Table 2 lists the rigorous enclosure) and to 74 digits in floating point. The integer relations behind Eq. (41) come from PSLQ on logarithms over $\{1, \log\pi, \log 2, \log 3, \log 5, \log 7, \log\Gamma(\frac{1}{4})\}$, with heights 4 and 15, unchanged between working precisions of 118 and 197 digits.

For the unipotent companions A_k of Eq. (46) we decomposed the continued period onto the local Frobenius basis at two matching radii and identified the coefficients by PSLQ. A recomputation at a third working precision with new matching radii gives coefficients that agree between the two radii to 77 digits (an internal consistency depth, distinct from the A_1 comparison of Table 2). PSLQ on a permuted basis padded with unrelated constants also returns the same relations, of height ≤ 24. A first pass at lower working precision had found the same two relations at 57 digits, but its planned higher-precision confirmation never ran, so we do not rely on it. Table 4 collects the bounds behind the statements of Secs. 3.4 and 4.3 that the complete two- and three-loop master integrals are analytic at the coalescence point and that certain logarithmic coefficients of ϖ_0 vanish.

We also tested whether the threshold coefficients can be extracted without integrating through the coalescence point, by fitting ϖ_0 at regular points to the values of the holomorphic Sym^{L-1}-of-sunrise solutions and reading off the fractional coefficient by PSLQ. Such a fit does not determine this coefficient to ≥ 30 digits at any of the four computed loop orders. Indeed, its agreement with ϖ_0 grows with basis size at the rate of Taylor interpolation (at four loops, from $8 \to 37$ digits over basis sizes $4 \to 16$, against $8 \to 29$ digits for bare monomials), and PSLQ returns only point-dependent relations with target coefficient zero. The obstruction is monotone up the four computed rungs, and we therefore integrate through the coalescence point in every case.

At three loops we also attempted a resurgence analysis in the spirit of ref. [56]. The holomorphic period there is Gevrey-0, a convergent series with geometric coefficient growth $\sim 36^n$, and hence there is no divergent series to which a Borel–Padé analysis could be applied. Moreover, a numerical continuation from the point of maximal unipotent monodromy to the coalescence point crosses three singular fibers ($t = 4, 16, 36$). No K3 boundary PSLQ match at ≥ 30 digits was obtained by that route.

object	data and method	quantity	bound
Complete two- and three-loop master integrals near the coalescence point, from fits to `AMFlow` *values*			
$(1,1,4)$ sunrise, master integral $I[1,1,1]$ (coefficient $M^{(0)}$ of Eq. (29))	ten points $t \in [-0.3, -10^{-5}]$ at $\sim$50 digits and an anchor at $t=-1$ at 110 digits; integer-power basis	prediction residual across increasing truncation orders	$1.9 \times 10^{-6} \to 1.1 \times 10^{-13}$
same	same	fitted $t^{1/4}$ coefficient	$\sim 3 \times 10^{-23}$ (bounded $< 1.8 \times 10^{-12}$)
same	same	fitted $t \log t$ coefficient	$\sim 10^{-12}$
same, orders ε^0 and ε^1	fractional basis against integer-power basis	prediction residual	6.7×10^{-3} and 1.0×10^{-2} against 2.8×10^{-8} and 2.3×10^{-8}; a logarithmic basis sits between the two
$(1,1,1,9)$ banana, master integral $I[1,1,1,1]$	nine points; integer-power basis against logarithmic basis	prediction residual	3×10^{-23} against 2×10^{-7}
same	same, at the best-determined order in ε	coefficient $b_{3/2}$ of $t^{3/2}$	$\lvert b_{3/2}\rvert \le 6.6 \times 10^{-30}$
Complete four-loop master at $d=2$, from the threshold expansion of ref. [64] about `AMFlow` *values at two Euclidean points*			
$(1,1,1,1,16)$ banana, master integral at $d=2$	threshold expansion [64]	coefficients of $t^{5/4}$, $t^{7/4}$; logarithmic tower	below 10^{-23}; absent
Maximal-cut periods at the coalescence point, from numerical continuation of the Picard–Fuchs operator			
$(1,1,1,9)$, ϖ_0	ball arithmetic	A_2 of Eq. (46)	below 10^{-156}
$(1,1,1,1,16)$, ϖ_0	linear decomposition onto the six local solutions, a hundred working digits	the two logarithmic coefficients	below 10^{-98}
same	same, 1400 bits, two paths and two matching radii	same	below 10^{-414}
same	ball arithmetic	same	below 10^{-89} (rigorous)

Table 4: Numerical bounds behind the statements that a fractional or logarithmic term is absent. Upper block: the complete two- and three-loop master integrals are regular at the coalescence point $t=0$ while the cut periods carry the fractional exponents (Sec. 3.4). Auxiliary-mass-flow values at Euclidean points approaching $t=0$ are fitted on the outer points in the stated local basis and the fit is compared with the points nearest $t=0$; an integer-power (analytic) basis is preferred over fractional and logarithmic ones by the margins shown, and the fitted non-analytic coefficients are bounded as listed. Middle block: the four-loop row records the bounds of ref. [64] on the fractional and logarithmic terms of the complete $(1,1,1,1,16)$ master at $d=2$, which is analytic at $t=0$ to that accuracy (Sec. 3.4). Lower block: the coefficients of the logarithmic local solutions in the threshold expansion of the holomorphic period vanish to the depth shown (Sec. 4.3). 'Ball arithmetic' marks rigorous enclosures; the other entries hold at the stated working precision. Mass labels $(M_1, \ldots, M_{L+1})$ are squared masses.

p	2	5	7	11	13	17	19	23	29	31	37	41	43	47	53
$\left(\frac{-15}{p}\right)$	+1	0	−1	−1	−1	+1	+1	+1	−1	+1	−1	−1	−1	+1	+1
$a_p(f_3)$	1	5	0	0	0	−14	−22	34	0	2	0	0	0	−14	−86
p	59	61	67	71	73	79	83	89	97	101	103	107	109	113	127
$\left(\frac{-15}{p}\right)$	−1	+1	−1	−1	−1	+1	+1	−1	−1	−1	−1	+1	+1	+1	−1
$a_p(f_3)$	0	−118	0	0	0	98	154	0	0	0	0	106	−22	−206	0
p	131	137	139	149	151	157	163	167	173	179	181	191	193	197	199
$\left(\frac{-15}{p}\right)$	−1	+1	+1	−1	+1	−1	−1	+1	+1	−1	+1	−1	−1	+1	+1
$a_p(f_3)$	0	226	−262	0	−238	0	0	−254	154	0	122	0	0	−374	−142

Table 5: Fourier coefficients a_p of the weight-three newform $f_3 = 15.3.\text{b.a}$ at the primes $p \le 199$ other than $p = 3$, with the Kronecker symbol $\left(\frac{-15}{p}\right)$. The coefficient vanishes exactly at the 23 primes inert in $\mathbb{Q}(\sqrt{-15})$, the CM law of Eq. (55); $p = 5$ is ramified. The toric point count of Eq. (119) gives the same a_p at each of the 44 primes $5 \le p \le 199$.

C.3 Integer-relation searches and point counts

All integer relations quoted in this paper were found with PSLQ and are unchanged between two working precisions. Each search was run together with a control search that recovers a known relation of the same kind at the same settings. We used 120 digits with coefficient bound 10^9 for the weight-three ring of Sec. 6.5, 10^8 for the classical ring searched with the ratio $T(-1)/\psi_1(-1)$, and 110 digits with 10^6 for the weight-four ring of Sec. 6.8. The boundary constants of Sec. 6 are thus PSLQ-negative against every named ring searched, at stated height with passing controls. For the sub-sector constants of the cone, by contrast, PSLQ finds relations: at 130 digits it returns $[1, 2, 0]$ on $[\text{bubble}^{-1}, \gamma_E, 1]$, $[-6, 12, 1, 0]$ on $[\text{bubble}^{0}, \gamma_E^2, \pi^2, 1]$, and the integer triple $(1, -2, 1)$ for the ε^{-2} coefficient of the tadpole.

Finally, we tested the CM pattern of Eq. (55) by a point count that does not use the q-expansion of f_3. The toric model of the equal-mass three-loop banana degenerates at the on-shell value of the modulus. We therefore count the $\mathbb{F}_p$-points $C(p)$ of a nearby non-degenerate fiber and find

$$C(p) \;=\; p^2 + 11 - 8p\,[\,p \equiv 2 \bmod 3\,] + a_p(f_3), \tag{119}$$

with $[\,\cdot\,]$ the indicator of the condition. The count obeys Eq. (119) with a_p the newform coefficient at every one of the 44 primes $5 \le p \le 199$ counted, and a_p vanishes at exactly the 23 inert primes among them (Table 5). It is a consistency cross-check, not a held-out arithmetic test of the on-shell motive: the count reproduces the CM pattern on a neighboring fiber, and Proposition 5.1 does not use it.

References

[1] Samuel Abreu, Ruth Britto, and Claude Duhr. The SAGEX review on scattering amplitudes, Chapter 3: Mathematical structures in Feynman integrals. 2022. arXiv:2203.13014, J. Phys. A **55** (2022) 443004.

[2] Luise Adams, Christian Bogner, and Stefan Weinzierl. The two-loop sunrise graph in two space-time dimensions with arbitrary masses in terms of elliptic dilogarithms. 2014. arXiv:1405.5640, J. Math. Phys. **55** (2014) 102301.

[3] Luise Adams, Christian Bogner, and Stefan Weinzierl. The two-loop sunrise integral around four space-time dimensions and generalisations of the Clausen and Glaisher functions towards the elliptic case. 2015. arXiv:1504.03255.

[4] Luise Adams and Stefan Weinzierl. Feynman integrals and iterated integrals of modular forms. 2017. arXiv:1704.08895.

[5] Luise Adams and Stefan Weinzierl. The ε-form of the differential equations for Feynman integrals in the elliptic case. 2018. arXiv:1802.05020, Phys. Lett. B **781** (2018) 270–278.

[6] Gert Almkvist and Duco van Straten. Calabi–Yau operators of degree two. 2021. arXiv:2103.08651, J. Algebraic Combin. **58** (2023).

[7] Tommaso Armadillo, Roberto Bonciani, Simone Devoto, Narayan Rana, and Alessandro Vicini. Evaluation of Feynman integrals with arbitrary complex masses via series expansions. *Comput. Phys. Commun.*, 282:108545, 2023. arXiv:2205.03345.

[8] S. Bauberger, F. A. Berends, M. Böhm, and M. Buza. Analytical and numerical methods for massive two-loop self-energy diagrams. 1995. arXiv:hep-ph/9409388, Nucl. Phys. B **434** (1995) 383–407.

[9] Konstantin Baune, Johannes Broedel, Egor Im, Artyom Lisitsyn, and Federico Zerbini. Schottky–Kronecker forms and hyperelliptic polylogarithms. 2024. arXiv:2406.10051, J. Phys. A **57** (2024) 445202.

[10] Marko Berghoff and Erik Panzer. Hierarchies in relative Picard–Lefschetz theory. 2022. arXiv:2212.06661.

[11] Spencer Bloch, Matt Kerr, and Pierre Vanhove. Local mirror symmetry and the sunset Feynman integral. 2017. arXiv:1601.08181, Adv. Theor. Math. Phys. **21** (2017) 1373–1453.

[12] Spencer Bloch and Pierre Vanhove. The elliptic dilogarithm for the sunset graph. 2015. arXiv:1309.5865, J. Number Theory **148** (2015) 328–364.

[13] Kilian Bönisch, Claude Duhr, Fabian Fischbach, Albrecht Klemm, and Christoph Nega. Feynman integrals in dimensional regularization and extensions of Calabi–Yau motives. 2021. arXiv:2108.05310, JHEP **09** (2022) 156.

[14] Kilian Bönisch, Fabian Fischbach, Albrecht Klemm, Christoph Nega, and Reza Safari. Analytic structure of all loop banana integrals. 2020. arXiv:2008.10574, JHEP **05** (2021) 066.

[15] Jonathan M. Borwein, Armin Straub, James Wan, and Wadim Zudilin. Densities of short uniform random walks. *Canad. J. Math.*, 64(5):961–990, 2012. With an appendix by Don Zagier. arXiv:1103.2995.

[16] Jacob L. Bourjaily et al. Functions beyond multiple polylogarithms for precision collider physics. 2022. arXiv:2203.07088, Snowmass 2021 white paper.

[17] J. B. Boyling. A homological approach to parametric Feynman integrals. *Il Nuovo Cimento A*, 53:351–375, 1968.

[18] D. J. Broadhurst, J. Fleischer, and O. V. Tarasov. Two-loop two-point functions with masses: asymptotic expansions and Taylor series, in any dimension. 1993. arXiv:hep-ph/9304303, Z. Phys. C **60** (1993) 287–302.

[19] David Broadhurst. Feynman integrals, L-series and Kloosterman moments. *Commun. Num. Theor. Phys.*, 10:527–569, 2016. arXiv:1604.03057.

[20] Johannes Broedel, Claude Duhr, Falko Dulat, Brenda Penante, and Lorenzo Tancredi. Elliptic symbol calculus: from elliptic polylogarithms to iterated integrals of Eisenstein series. 2018. arXiv:1803.10256, JHEP **08** (2018) 014.

[21] Johannes Broedel, Claude Duhr, Falko Dulat, Brenda Penante, and Lorenzo Tancredi. Elliptic Feynman integrals and pure functions. 2019. arXiv:1809.10698, JHEP **01** (2019) 023.

[22] Johannes Broedel, Claude Duhr, Falko Dulat, and Lorenzo Tancredi. Elliptic polylogarithms and iterated integrals on elliptic curves. part i: general formalism. 2017. arXiv:1712.07089, JHEP **05** (2018) 093; see also 1712.07095 (part II: sunrise).

[23] Johannes Broedel, Claude Duhr, and Nils Matthes. Meromorphic modular forms and the three-loop equal-mass banana integral. 2021. arXiv:2109.15251, JHEP **02** (2022) 184.

[24] Simon Caron-Huot and Johannes M. Henn. Iterative structure of finite loop integrals. 2014. arXiv:1404.2922, JHEP **06** (2014) 114 (App. A + ancillary `Amatrix29D.txt`).

[25] Kuo-Tsai Chen. Iterated path integrals. *Bull. Amer. Math. Soc.*, 83(5):831–879, 1977.

[26] M. Correia, M. Giroux, and S. Mizera. SOFIA: Singularities of Feynman integrals automatized. 2025. arXiv:2503.16601.

[27] Leonardo de la Cruz and Pierre Vanhove. Algorithm for differential equations for Feynman integrals in general dimensions. 2024. arXiv:2401.09908.

[28] Charles F. Doran, Andrew Harder, Eric Pichon-Pharabod, and Pierre Vanhove. Motivic geometry of two-loop Feynman integrals. *Quart. J. Math.*, 75(3):901–967, 2024.

[29] Claude Duhr. Mathematical aspects of scattering amplitudes. 2015. arXiv:1411.7538, TASI 2014 lectures, in: Journeys Through the Precision Frontier (WSP, 2015) 419–476.

[30] Claude Duhr. Modular forms for three-loop banana integrals. 2025. arXiv:2502.15325.

[31] Claude Duhr and Sara Maggio. Feynman integrals, elliptic integrals and two-parameter K3 surfaces. 2025. arXiv:2502.15326.

[32] Claude Duhr and Sara Maggio. Three-loop banana integrals with three equal masses. 2025. arXiv:2511.19245.

[33] Claude Duhr, Sara Maggio, Franziska Porkert, Cathrin Semper, and Sven F. Stawinski. Three-loop banana integrals with four unequal masses. 2025. arXiv:2507.23061, JHEP **12** (2025) 034.

[34] Martin Eichler. Eine Verallgemeinerung der Abelschen Integrale. 1957. Math. Z. **67** (1957) 267–298.

[35] Claudia Fevola, Sebastian Mizera, and Simon Telen. Principal Landau determinants. 2023. arXiv:2311.16219, Comput. Phys. Commun. **303** (2024) 109278; see also 2311.14669.

[36] Hjalte Frellesvig. On epsilon factorized differential equations for elliptic feynman integrals. 2021. arXiv:2110.07968.

[37] Alexander B. Goncharov. Multiple polylogarithms and mixed Tate motives. 2001. arXiv:math/0103059.

[38] Alexander B. Goncharov, Marcus Spradlin, C. Vergu, and Anastasia Volovich. Classical polylogarithms for amplitudes and Wilson loops. 2010. arXiv:1006.5703, Phys. Rev. Lett. **105** (2010) 151605.

[39] S. Groote, J. G. Körner, and A. A. Pivovarov. On the evaluation of sunset-type Feynman diagrams. *Nucl. Phys. B*, 542:515–547, 1999. arXiv:hep-ph/9806402.

[40] S. Groote and A. A. Pivovarov. Threshold expansion of Feynman diagrams within a configuration space technique. *Nucl. Phys. B*, 580:459–484, 2000. arXiv:hep-ph/0003115.

[41] Holmfridur S. Hannesdottir, Andrew J. McLeod, Matthew D. Schwartz, and Cristian Vergu. Constraints on sequential discontinuities from the geometry of on-shell spaces. *JHEP*, 07:236, 2023.

[42] Johannes M. Henn. Multiloop integrals in dimensional regularization made simple. 2013. arXiv:1304.1806, Phys. Rev. Lett. **110** (2013) 251601.

[43] Johannes M. Henn. Lectures on differential equations for Feynman integrals. *J. Phys. A*, 48:153001, 2015.

[44] Martijn Hidding. DiffExp, a Mathematica package for computing Feynman integrals in terms of one-dimensional series expansions. *Comput. Phys. Commun.*, 269:108125, 2021. arXiv:2006.05510.

[45] Fredrik Johansson. Arb: efficient arbitrary-precision midpoint-radius interval arithmetic. *IEEE Transactions on Computers*, 66:1281–1292, 2017.

[46] Jonas Klappert, Fabian Lange, Philipp Maierhöfer, and Johann Usovitsch. Integral reduction with Kira 2.0 and finite-field methods. 2021. arXiv:2008.06494, Comput. Phys. Commun. **266** (2021) 108024.

[47] Albrecht Klemm, Christoph Nega, and Reza Safari. The l-loop banana amplitude from GKZ systems and relative Calabi–Yau periods. 2019. arXiv:1912.06201, JHEP **04** (2020) 088.

[48] Albrecht Klemm and Stefan Theisen. Considerations of one modulus Calabi–Yau compactifications: Picard–Fuchs equations, Kähler potentials and mirror maps. 1993. arXiv:hep-th/9205041, Nucl. Phys. B **389** (1993) 153–180.

[49] Kunihiko Kodaira. On compact analytic surfaces. II. *Ann. of Math. (2)*, 77:563–626, 1963.

[50] Pierre Lairez and Pierre Vanhove. Algorithms for minimal Picard–Fuchs operators of Feynman integrals. *Lett. Math. Phys.*, 113(2):37, 2023.

[51] P. V. Landshoff, D. I. Olive, and J. C. Polkinghorne. The hierarchical principle in perturbation theory. *Il Nuovo Cimento A*, 43:444–453, 1966.

[52] S. Laporta and E. Remiddi. Analytic treatment of the two-loop equal-mass sunrise graph. 2005. arXiv:hep-ph/0406160, Nucl. Phys. B **704** (2005) 349–386.

[53] Xiao Liu and Yan-Qing Ma. AMFlow: a Mathematica package for Feynman integrals computation via auxiliary mass flow. 2022. arXiv:2201.11669; package amflow; amflow-cpp github.com/chang18/amflow-cpp.

[54] Ron Livné. Motivic orthogonal two-dimensional representations of $\mathrm{Gal}(\bar{\mathbb{Q}}/\mathbb{Q})$. *Israel J. Math.*, 92:149–156, 1995.

[55] Sara Maggio and Yoann Sohnle. On canonical differential equations for Calabi–Yau multi-scale Feynman integrals. 2025. arXiv:2504.17757, JHEP **10** (2025) 202.

[56] Eleanor McSpirit and Larry Rolen. Quantum modular forms and resurgence. 2025. arXiv:2505.00799.

[57] Hildegard Müller and Stefan Weinzierl. A Feynman integral depending on two elliptic curves. *JHEP*, 07:101, 2022. arXiv:2205.04818.

[58] Sebastian Pögel, Xing Wang, and Stefan Weinzierl. Taming Calabi–Yau Feynman integrals: the four-loop equal-mass banana integral. 2022. arXiv:2211.04292, Phys. Rev. Lett. **130** (2023) 101601.

[59] Sebastian Pögel, Xing Wang, and Stefan Weinzierl. The three-loop equal-mass banana integral in ε-factorised form with meromorphic modular forms. 2022. arXiv:2207.12893, JHEP **09** (2022) 062.

[60] Sebastian Pögel, Toni Teschke, Xing Wang, and Stefan Weinzierl. The unequal-mass three-loop banana integral. 2025. arXiv:2507.23594.

[61] Ettore Remiddi and Lorenzo Tancredi. Differential equations and dispersion relations for Feynman amplitudes. The two-loop massive sunrise and the kite integral. 2016. arXiv:1602.01481, Nucl. Phys. B **907** (2016) 400–444.

[62] A. Sabry. Fourth order spectral functions for the electron propagator. 1962. Nucl. Phys. **33** (1962) 401–430.

[63] Matthew D. Schwartz. Automated computation of Feynman integrals with BootLoops, 2026. companion paper, https://bootloops.ai/FeynmanBootstrap.pdf.

[64] Matthew D. Schwartz. Polylogarithmic, elliptic, and Calabi–Yau Feynman integrals from a hybrid bootstrap, 2026. companion paper, https://bootloops.ai/SmatrixBootLoops.pdf.

[65] Atle Selberg and Sarvadaman Chowla. On Epstein's zeta-function. *J. Reine Angew. Math.*, 227:86–110, 1967.

[66] Vladimir A. Smirnov. *Analytic Tools for Feynman Integrals*, volume 250 of *Springer Tracts in Modern Physics*. Springer, 2012.

[67] Matija Tapušković. The cosmic Galois group, the sunrise Feynman integral, and the relative completion of $\Gamma_1(6)$. 2023. arXiv:2303.17534.

[68] Duco van Straten. Calabi–Yau operators. 2017. arXiv:1704.00164.

[69] Stefan Weinzierl. *Feynman Integrals: A Comprehensive Treatment for Students and Researchers*. UNITEXT for Physics. Springer, 2022. arXiv:2201.03593, Springer (2022), DOI 10.1007/978-3-030-99558-4.

[70] Matthias Wilhelm and Chi Zhang. Symbology for elliptic multiple polylogarithms and the symbol prime. 2022. arXiv:2206.08378, JHEP **01** (2023) 089.

[71] Feiyu Yang, Jianyu Gong, and Yang Zhang. Genus drop involving non-hyperelliptic curves in Feynman integrals. 2026. arXiv:2605.07729.